Available online at www.sciencedirect.com

ScienceDirect

Geochimica et Cosmochimica Acta 165 (2015) 484–500

Geochimica et Cosmochimica Acta

www.elsevier.com/locate/gca

Zirconium isotope evidence for the heterogeneous distribution of s-process materials in the solar system

W. Akram [a,b,1,*], M. Schönbächler [a,b,1], S. Bisterzo [c], R. Gallino [c]

[a] School of Earth, Atmospheric and Environmental Sciences, The University of Manchester, Oxford Road, Manchester M13 9PL, UK
[b] Institute for Geochemistry and Petrology, ETH, Clausiusstrasse 25, 8092 Zürich, Switzerland
[c] Dipartimento di Fisica, Università di Torino, Via P. Giura 1, I–10125 Torino, Italy

Received 11 April 2014; accepted in revised form 15 February 2015; available online 24 February 2015

Abstract

A growing number of elements show well-resolved nucleosynthetic isotope anomalies in bulk-rock samples of solar system materials. In order to establish the occurrence and extent of such isotopic heterogeneities in Zr, and to investigate the origin of the widespread heterogeneities in our solar system, new high-precision Zr isotope data are reported for a range of primitive and differentiated meteorites. The majority of the carbonaceous chondrites (CV, CM, CO, CK) display variable ε^{96}Zr values ($\leqslant$1.4) relative to the Earth. The data indicate the heterogeneous distribution of ^{96}Zr-rich CAIs in these meteorites, which sampled supernova (SN) material that was likely synthesized by charged-particle reactions or neutron-captures. Other carbonaceous chondrites (CI, CB, CR), ordinary chondrites and eucrites display variable, well-resolved ^{96}Zr excesses correlated with potential, not clearly resolved variations in ^{91}Zr relative to the bulk–Earth and enstatite chondrites. This tentative correlation is supported by nucleosynthetic models and provides evidence for variable contributions of average solar system s-process material to different regions of the solar system, with the Earth representing the most s-process enriched material. New s-process model calculations indicate that this s-process component was produced in both low and intermediate mass asymptotic giant branch (AGB) stars. The isotopic heterogeneity pattern is different to the s-process signature resolved in a previous Zr leaching experiment, which was attributed to low mass AGB stars. The bulk-rock heterogeneity requires several nucleosynthetic sources, and therefore opposes the theory of the injection of material from a single source (e.g., supernova, AGB star) and argues for a selective dust-sorting mechanism within the solar nebula. Thermal processing of labile carrier phases is considered and, if correct, necessitates the destruction and removal of non-s-process material from the innermost solar system. New Zr isotope data on mineral separates and a fusion crust sample from chondrites indicate that this non-s-process material could be silicates.

1. INTRODUCTION

Mass–independent, nucleosynthetic isotope variations are identified across a range of presolar grains and refractory inclusions (e.g. Ca–Al rich inclusions (CAIs)) that reside in primitive meteorites (e.g., Birck, 2004; Lauretta and McSween, 2006). These distinct chemical and isotopic compositions, relative to that of the average solar system, are thought to reflect (i) the nucleosynthetic signatures of the stellar environments in which these grains were

* Corresponding author at: Institute for Geochemistry and Petrology, ETH, Clausiusstrasse 25, 8092 Zürich, Switzerland. Tel.: + 41 44 632 6869.
E-mail address: waheed.akram@erdw.ethz.ch (W. Akram).
[1] Present address: Institute for Geochemistry and Petrology, ETH, Clausiusstrasse 25, 8092 Zürich, Switzerland.

http://dx.doi.org/10.1016/j.gca.2015.02.013
0016-7037/

produced (Anders and Zinner, 1993) or (ii) the local composition of the solar nebula from which the refractory inclusions (e.g. CAIs) formed prior to planetary differentiation.

In addition, evidence exists for planetary-scale, mass-independent isotope heterogeneities in bulk carbonaceous chondrites relative to other meteorites, the Moon and Earth for several elements – O (Clayton, 1993; Clayton and Mayeda, 1999), Ca (Simon et al., 2009; Chen et al., 2011), Ti (Niemeyer and Lugmair, 1984; Leya et al., 2008; Trinquier et al., 2009; Zhang et al., 2012), Cr (Rotaru et al., 1992; Podosek et al., 1997; Lugmair and Shukolyukov, 2001; Trinquier et al., 2007), Ni (Regelous et al., 2008; Steele et al., 2012), Mo (Dauphas et al., 2002a; Chen et al., 2004; Burkhardt et al., 2011), Ru (Chen et al., 2010), Ba (Ranen and Jacobsen, 2006; Carlson et al., 2007), Nd (Andreasen and Sharma, 2006) and Sm (Andreasen and Sharma, 2006, 2007). In contrast, homogeneous isotopic compositions are observed for Te (Fehr et al., 2006), Hf (Sprung et al., 2010), Zn (Moynier et al., 2009) and Os (Brandon et al., 2005; Yokoyama et al., 2007, 2010; van Acken et al., 2011). These observations are consistent with the idea that isotopic anomalies are generally limited to refractory elements (Clayton et al., 1988). The exact origin(s) of these isotopic heterogeneities remain(s) unclear, however. These variations represent preserved nucleosynthetic isotope signatures that are unrelated to the effects of galactic cosmic ray spallation and radioactive decay. There are currently two general interpretations to explain these isotopic heterogeneities.

The first envisages that they are due to the heterogeneous distribution of isotopically anomalous carrier phases in the solar system. For example, the ^{50}Ti variations in carbonaceous chondrites scale with the abundance of CAIs (Leya et al., 2008, 2009), whereas those of ^{54}Cr may relate to nanometer sized spinel grains produced in presolar, supernova environments (Dauphas et al., 2010; Qin et al., 2011). Furthermore, the enrichment of neutron–rich isotopes (^{50}Ti, ^{54}Cr) in carbonaceous chondrites and CAIs, along with their possible coupling with short–lived radionuclides (e.g. ^{60}Fe), suggest the co-production of these isotopes in explosive stellar environments (e.g., Quitté et al., 2007). These variations are generally attributed to the occurrence of a nearby supernova, which injected material into our solar system that was subsequently incompletely admixed (e.g., Foster and Boss, 1996). The injection may also have caused the collapse of the molecular cloud that initiated the formation of our solar system (Cameron and Truran, 1977).

The second interpretation for the origin of these isotopic heterogeneities implies that the variations are the result of thermal processes, acting on an initial dust cloud containing presolar carriers, which was on average isotopically homogeneous. Gas-dust, or dust–dust separation processes act on the system, after the preferential vaporisation of thermally unstable phases (Huss et al., 2003), which generate the isotopic heterogeneities (e.g., Trinquier et al., 2009). For example, the correlated isotopic variability of ^{46}Ti and ^{50}Ti (both reside in different carriers, and are produced by different nucleosynthetic pathways, Clayton, 2003; Trinquier et al., 2009; Zhang et al., 2012) in the solar system exclude a single carrier phase as the cause.

Whether these isotopic heterogeneities are generated through the addition and incomplete mixing of anomalous carrier phases, or the removal of such carriers by processing in the solar nebula, has a profound implication on the origin of our solar system. The heterogeneities provide important information about nucleosynthesis in stars, the astrophysical environment (stellar neighbourhood) in which our solar system formed, and the subsequent processing of disk material during the early evolution of the solar system.

The analysis of Zr isotopes provides further insight into the origin of isotopic heterogeneities in the inner solar system. Zirconium is a highly refractory element ($T_c = 1753$ K: 50% condensation temperature at 10^{-4} bar; Lodders, 2003) and therefore rather insensitive to the thermal processes that occurred in the early solar system and affected the elemental budgets of volatile elements. All five stable isotopes are mainly produced by s(low)- and r(apid)-neutron-capture processes, which allow them to track the mixing of different neutron–rich nucleosynthetic components in the solar nebula. The majority of the observed solar system abundances of ^{90}Zr (85%), ^{91}Zr (106%), ^{92}Zr (100%) and ^{94}Zr (126%) are accounted for by the s-process (Bisterzo et al., 2011b). Multiple nucleosynthetic pathways and stellar sources, however, contribute to the synthesis of ^{96}Zr. Depending on how various s-process contributions from low mass (LM) and intermediate mass (IM) asymptotic giant branch (AGB) stars are integrated, these models can account for 51% (Bisterzo et al., 2011b) or 82% (Travaglio et al., 2004) of the ^{96}Zr solar system abundance. In such neutron-capture environments, the ^{96}Zr production strongly depends on the neutron density during nucleosynthesis because of the relatively short beta–decay half–life of ^{95}Zr ($T_{½} \sim 64$ days). The remaining ^{96}Zr production is attributed to charged-particle reactions (CPRs), and to a lesser extent, the r-process (Cameron, 1973; Käppeler et al., 1989; Farouqi et al., 2010; Akram et al., 2013), which are largely insensitive to the ^{95}Zr half-life. These processes likely take place in the inner mass shells or the high entropy, neutrino–driven winds of core–collapse supernovae, respectively (Kratz et al., 2008; Wasserburg and Qian, 2009). However, other possibilities include a high neutron density (>10^8 neutrons/cm^3) s–process occurring in IM (5–8 $M_\odot$) AGB stars (Travaglio et al., 2004), neutron bursts in supernovae (Meyer et al., 2000), and co-production alongside p-isotopes in thermonuclear explosions of type Ia supernovae (Travaglio et al., 2011). Consequently, the r-residual method (i.e. r-process abundance = solar system abundance – s-process abundance, e.g. Arlandini et al., 1999) cannot be directly applied to Zr, and other light elements (e.g. Qian and Wasserburg, 2007), in order to determine the r-process contributions (e.g. Bisterzo et al., 2011b).

Primitive meteorites show evidence for nucleosynthetic ^{96}Zr isotope variations. For example, refractory inclusions from the CV3 chondrite Allende exhibit clearly resolved excesses in ^{96}Zr (Harper et al., 1991; Schönbächler et al., 2003; Akram et al., 2013) relative to the terrestrial standard.

A recent study (Akram et al., 2013) reports that the majority of the analysed CAIs (75%) are characterised by relatively uniform enrichments in $^{96}Zr/^{90}Zr$ ($\varepsilon^{96}Zr = 1.90 \pm 0.09$), with some scatter. This ^{96}Zr enrichment is coupled with ^{50}Ti excesses (and potentially other neutron–rich isotopes of the Fe group elements) and depletions in the r–process Hf isotopes (Akram et al., 2013). Collectively, the data point to CAIs sampling material from the ejecta of a core–collapse, type II supernova, which was synthesized via CPRs (Akram et al., 2013). Moreover, the same study identified ^{96}Zr enrichments for bulk-rock samples of Murchison (CM2), Dar al Gani 137 (CO) and Dar al Gani 275 (CK), which were hinted at, but not entirely resolved for CV and CM meteorites previously (Schönbächler et al., 2004, 2005).

The aim of this study is to (i) characterise the extent of nucleosynthetic Zr isotope anomalies in a wide–range of bulk–rock planetary material, (ii) identify the corresponding carrier phases and (iii) understand the nucleosynthetic origin of the Zr isotope heterogeneities with updated stellar models. To this end, we present new high–precision Zr isotope measurements for eucrites, enstatite, ordinary and carbonaceous chondrites. The study also addresses the question of whether the heterogeneities are due to (i) presolar dust injected into the solar nebula, or instead (ii) processes within the solar nebula such as thermal processing or grain sorting.

2. ANALYTICAL TECHNIQUES

High–precision Zr isotope data are presented for 2 zircons (zircon (50) Jack Hills, Australia, 4.01 Ga and zircon (41), Jack Hills, Australia, 3.4 Ga; Amelin et al., 1999; Schönbächler et al., 2004), 3 terrestrial standard rocks (USGS BHVO-2, SCo-1 and AGV-2), 12 carbonaceous chondrites, 4 ordinary chondrites, 2 enstatite chondrites and 5 basaltic eucrites in addition to mineral separates from chondrites. While the terrestrial samples came as solutions (zircons) or powders (USGS rocks), meteorites were obtained as chips. Sample chips were treated with ethanol in an ultrasonic bath (5 min), except for carbonaceous chondrites, which are too porous for this treatment. Where present, fusion crust and weathered components were removed. The samples were subsequently powdered in an aluminium oxide mortar and pestle.

Up to 1 g whole-rock chondrite, 30–60 mg eucrite and 100–400 mg terrestrial rocks were dissolved. An assortment of chondrules, of various sizes (100 μm–1 mm) weighing approximately 111 mg were hand-separated from Allende (CV3) using tweezers. For Renazzo (CR2), a clean chip (200 mg) and several fusion crust dominated fragments (100 mg) were separated and processed separately. The preparation of the metal–rich whole-rock fraction of Renazzo and mineral separates of Forest Vale (H4) and Hvittis (EL6) are described elsewhere (Lee and Halliday, 2000; Schönbächler et al., 2003).

High-purity acids (<5 ppt Zr) and solvents were used throughout this study to minimise the procedural blank. Commercially available analytical reagent grade HCl and HNO_3 were purified using a sub–boiling distillation quartz still. Trace element grade H_2SO_4 (Fisher Scientific Optima brand), HF (Romil UltraPure), H_2O_2 (Fluka Sigma Aldrich Select grade) and deionised water (18.2 MΩ·cm) from a Milli-Q purification system were used.

Zirconium fractions from the zircons (50) and (41) were available from a previous study (Schönbächler et al., 2004). Different powdered masses of BHVO-2 (100, 200, 300 mg) and SCo-1 (200, 300, 400 mg) were dissolved with concentrated HF-HNO_3 in a Parr© acid digestion vessel (bomb) or microwave, following the procedure of Schönbächler et al. (2004) and Akram et al. (2013), respectively. All powdered meteorite samples were digested, up to 300 mg at a time, in a Parr© bomb. Metal–rich samples (Bencubbin, Forest Vale, St. Severin, Abee and Indarch) were digested on a hotplate in 5 ml 6 M HNO_3 (120 °C, 48 h) before the Parr© bomb digestion. The chemical separation of Zr from the sample matrix was based on the two–stage anion exchange technique developed by Schönbächler et al. (2004), with some modifications (Table 1). The first ion exchange column separation follows Schönbächler et al. (2004), but is scaled up for processing up to 1 g of rock powder. It also substitutes one column volume of 3 M HCl–10 M HF with two column volumes of 0.5 M HCl for the resin cleaning stage. For the second ion exchange column, the "matrix elution 2" and "matrix elution 3" steps were added to avoid the elution of H_2SO_4 into the Zr fraction, which is hazardous to the desolvating nebulizer used for sample analyses. The isotopic analyses were carried out on a Nu Plasma multiple collector–inductively coupled plasma mass spectrometer (MC–ICPMS) coupled with a Cetac Aridus II nebulizer sample introduction system utilising a self–aspirating Aspire (100 μL/min) PFA nebulizer. Following Schönbächler et al. (2004), all five Zr isotopes were analysed simultaneously on Faraday collectors (with 10^{11} Ω resistors). The ion beam intensities were normalised to the ^{90}Zr signal and corrected for instrumental mass fractionation relative to $^{94}Zr/^{90}Zr$ (=0.3381; Minster and Allègre, 1982) using the exponential law. Individual sample measurements consisted of 5 s integration, repeated 60 times. Electronic baselines were measured before each analysis for 15s and subtracted. Additional isotopes (^{95}Mo, ^{99}Ru) were also measured during each analysis to correct for isobaric interferences on ^{92}Zr (^{92}Mo), ^{94}Zr (^{94}Mo) and ^{96}Zr (^{96}Mo, ^{96}Ru), over two cycles: cycle 1: mass 90–96; cycle 2: mass 95–101. A 2% aliquot of each sample solution was screened prior to isotopic analysis to ensure that the signal intensities of interfering isobars ($^{94,96}Mo$, ^{96}Ru) and argides ($^{50}Ti^{40}Ar$, $^{51}V^{40}Ar$, $^{52}Cr^{40}Ar$, $^{54}Fe^{40}Ar$) were within the acceptable limits ($Mo/Zr \leqslant 0.001$, $Ru/Zr \leqslant 0.01$, $Ti/Zr \leqslant 1$, $V/Zr \leqslant 0.3$, $Cr/Zr \leqslant 0.3$, $Fe/Zr \leqslant 0.9$; Schönbächler et al., 2004). If these limits were exceeded, the ion exchange procedure was repeated to remove the interfering element(s). The applied interference corrections (Mo, Ru) on $\varepsilon^{91}Zr$, $\varepsilon^{92}Zr$ and $\varepsilon^{96}Zr$ were less than 1, 10 and 60 ε, respectively. Depending on the daily sensitivity, 200–400 ng Zr (solutions ran at 200 ppb Zr) was required per measurement and yielded total Zr ion beam intensities between 2.5×10^{-10} A to 3.5×10^{-10} A. All samples were bracketed by a Zr Alfa Aesar single element standard solution (#63–061671G) at ion beam intensities that were

Table 1
Ion exchange chemistry for the separation of Zr fom Ti.

	Ion exchange 1:			Ion exchange 2:		
Step	Volume (mL)	Acid/resin	Elements eluted	Volume (mL)	Acid/resin	Elements eluted
Resin	3.5	BioRad AG1–X8, Cl^- form	–	0.7	BioRad AG1–X8, Cl^- form	–
Resin cleaning	60	0.5 M HCl	–	18	0.5 M HCl	–
	30	6 M HCl + 1 M HF	–	9	6 M HCl + 1 M HF	–
	30	H_2O	–	9	H_2O	–
Pre-conditioning	30	4 M HF	–	8	0.25 M H_2SO_4 + 1% H_2O_2	–
Sample loading	12	4 M HF	–	1.5	0.25 M H_2SO_4 + 1% H_2O_2	–
Matrix elution 1	30	4 M HF	Mg, Ca, Cr, Fe, Ni, Ru	8	0.25 M H_2SO_4 + 1% H_2O_2	Fe, Ti, Cr
Matrix elution 2	–	–	–	2	0.5 M HCl + 0.5 M HF	Zr (<10%)
Matrix elution 3	–	–	–	0.3	6 M HCl + 1 M HF	–
Zr elution	10	6 M HCl + 1 M HF	Ti, Zr, Hf, Th	1.7	6 M HCl + 1 M HF	Zr, Hf
Post Zr elution	10	6 M HCl + 1 M HF	W	3	6 M HCl + 1 M HF	–
Mo elution	30	3 M HNO_3	Mo	–	–	–

matched to better than 20%. The isotopic data are reported using the epsilon notation, ε – the deviation of the sample from the Alfa Aesar standard solution in parts per ten thousand, normalised to $^{94}Zr/^{90}Zr$.

3. RESULTS

3.1. Terrestrial rocks: accuracy and reproducibility of the Zr isotope analyses

Four different digestions of the basalt BHVO-2 were analysed and complemented by 3 digestions of the shale SCo-1. These digestions were treated separately through the ion exchange procedure (a total of 8 different treatments; Table 2). The Zr sample solutions were analysed over a period of 2 years relative to the Alfa Aesar standard solution. The combined results yield a 2σ standard deviation of ±13 ppm ($\varepsilon^{91}Zr$), ±11 ppm ($\varepsilon^{92}Zr$) and ±27 ppm ($\varepsilon^{96}Zr$). Furthermore, independent analyses from 2 zircons and the andesite AGV-2 are also reported (Table 2). Including these data yields a 2σ standard deviation of ±15 ppm ($\varepsilon^{91}Zr$), ±15 ppm ($\varepsilon^{92}Zr$) and ±25 ppm ($\varepsilon^{96}Zr$). Within this precision, all terrestrial samples (BHVO-2, SCo-1, AGV-2, zircons (50) and (41)) display Zr isotope compositions identical to the Alfa Aesar synthetic Zr solution (Table 2, Fig. 1), which demonstrates the accuracy of the data. The improved precision obtained here compared to previous work (Schönbächler et al. 2002, 2003, 2004, 2005) (±30 ppm ($\varepsilon^{91}Zr$), ±20 ppm ($\varepsilon^{92}Zr$) and ±80 ppm ($\varepsilon^{96}Zr$)) was achieved by (i) measuring sample solutions multiple times to improve the statistics and (ii) applying higher ion beam intensities, which was possible by increasing the original 10 V dynamic range of the NuPlasma Faraday collector to 20 V for ^{90}Zr by coupling two 10^{11} Ω resistors.

The 2σ standard deviation of the terrestrial samples provides a good estimate for the *long term reproducibility* of the Zr isotope measurements. This estimate is based on independent sample analyses and takes into account samples with varying sample matrices. It assumes that all terrestrial samples possess an identical Zr isotope composition and therefore, the reported 2σ standard deviation represents a conservative upper limit for the sample reproducibility. For sample analyses obtained on single sample digestions consisting of a number of measurements (n) $\leqslant$4, this external *long term* reproducibility is assigned as the uncertainty of the analysis (Table 3), unless the individual sample error was larger. The individual sample error was estimated by propagating the internal error (2σ standard error of the mean based on 60 5 s integrations) with the external reproducibility (2σ standard deviation) of the bracketing standards. As such, the individual sample error provides an estimate that considers both the internal and external uncertainty. For the terrestrial samples (Table 2, Fig. 1) with $n \geqslant 4$ analyses, the weighted average ($X_w = \sum_i^n x_i \cdot w_i / \sum_i^n w_i$; sample measurements x_i, weights w_i) of each sample aliquot overlaps with the mean of all terrestrial samples within the uncertainty of the weighted average ($1/\sqrt{\sum_i^n w_i}$; 2σ) reflecting the standard error ($2SD/\sqrt{n}$). The exception is the aliquot BHVO-2 (1), where the $\varepsilon^{91}Zr$ and $\varepsilon^{92}Zr$ do not overlap with the terrestrial

Table 2
Zirconium isotope compositions of terrestrial samples.

Sample	Type	Mass[♯] (g)	Digest	ε^{91}Zr	ε^{92}Zr	ε^{96}Zr	*N*
BHVO-2 (1)	Basalt	0.10	MW	−0.21 ± 0.06	−0.15 ± 0.06	0.23 ± 0.18	4
BHVO-2 (2)	Basalt	0.20	MW	−0.01 ± 0.08	−0.01 ± 0.06	0.18 ± 0.12	4
BHVO-2 (3)	Basalt	0.30	MW	−0.08 ± 0.11	−0.13 ± 0.06	0.36 ± 0.21	2
BHVO-2 (4)	Basalt	0.20	PB	−0.08 ± 0.10	0.04 ± 0.07	0.08 ± 0.14	4
BHVO-2 mean				−0.12 ± 0.04	−0.08 ± 0.03	0.19 ± 0.08	
SCo-1 (1)	Shale	0.30	MW	−0.07 ± 0.03	−0.05 ± 0.03	0.07 ± 0.07	18
SCo-1 (2a)	Shale	0.40	MW	0.01 ± 0.07	−0.02 ± 0.07	−0.02 ± 0.09	4
SCo-1 (2b)	Shale	0.40	MW	−0.06 ± 0.04	−0.11 ± 0.03	−0.06 ± 0.09	19
SCo-1 (3)	Shale	0.20	PB	−0.05 ± 0.05	−0.01 ± 0.05	0.11 ± 0.12	11
SCo-1 mean				−0.06 ± 0.02	−0.06 ± 0.02	0.02 ± 0.04	
AGV-2[a]	Andesite	–	PB	−0.09 ± 0.10	−0.01 ± 0.11	0.22 ± 0.30	2
Zircon 50 [b]	Zircon	–	–	0.09 ± 0.12	0.05 ± 0.15	−0.01 ± 0.34	3
Zircon 41 [b]	Zircon	–	–	−0.02 ± 0.11	0.08 ± 0.11	0.11 ± 0.41	2
Earth mean				−0.07 ± 0.02	−0.06 ± 0.02	0.06 ± 0.04	73

The weighted mean and its associated uncertainty (2σ) are given for repeat measurements. The weighted mean (and its associated uncertainty) of each digest is used to define the sample means for multiple digests, whereas the final Earth mean is calculated using measurements of every digest (i.e. n = 11). Data include samples digested in the microwave (MW) and Parr bomb (PB). Numbers in parentheses denote digest number, whereas different sample splits over the columns are designated with the letters *a*, *b*. Sample information available from: [a] Sprung et al. (2010), [b] Schönbächler et al. (2002) and references within.

[♯] Total sample mass powdered from which an aliquot was consumed for digestion and MC–ICPMS analyses.

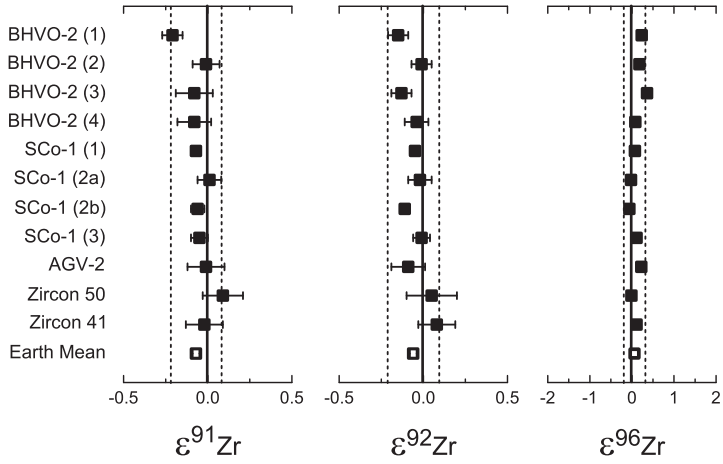

Fig. 1. Zirconium isotope compositions of terrestrial samples. The weighted average, and its associated uncertainties (2σ) are displayed. Numbers in parentheses indicate different digests. Open symbol denotes the weighted average of all terrestrial samples. Dashed lines indicate the external reproducibility – the 2σ standard deviation derived from the 73 analyses of the terrestrial rock standards. Data for AGV-2 from Akram et al. (2013).

mean within the uncertainty of the weighted average. However, BHVO-2 (1) was the first sample analysed in this study and its chemical separation did not include the improvements implemented afterwards that minimize traces of sulphuric acid in the analysed Zr fraction. Therefore, for samples with 4 or more measurements ($n \geqslant 4$, Table 3), the weighted mean and its associated uncertainty are shown.

3.2. Whole-rock carbonaceous, ordinary and enstatite chondrites, and basaltic eucrites

3.2.1. Carbonaceous chondrites

This group reveals the largest spread in ε^{96}Zr values. The CI meteorite Orgueil displays a slight excess ($\varepsilon^{96}\text{Zr} = 0.30 \pm 0.22$; Table 3) relative to the Zr standard solution, but is in agreement with previous work ($\varepsilon^{96}\text{Zr} = -0.1 \pm 1.5$; Schönbächler et al., 2003; 2005). The data point just overlaps, within uncertainties, with the terrestrial rock standards (Tables 2 and 3). The CV3 chondrites show the largest enrichment on average ($\varepsilon^{96}\text{Zr} = 1.17 \pm 0.17$). In particular, Allende (CV3) displays a well–resolved positive ε^{96}Zr of 1.21 ± 0.19 (Table 3), which was indicated but not clearly resolved previously (ε^{96}Zr of 1.00 ± 0.82; Schönbächler et al., 2003). The ε^{91}Zr data for Orgueil (CI), Elephant Moraine (CR), Renazzo (CR) and Bencubbin (CB) are consistently more negative than the Alfa Aesar Zr solution, however, they overlap with the average defined by the terrestrial samples (Table 2). For further discussion and the identification of

Table 3
Zirconium isotope compositions of whole-rock samples and mineral separates.

Sample	Specimen No./Fraction	Type	Mass[‡] (g)	$\varepsilon^{91}Zr$	$\varepsilon^{92}Zr$	$\varepsilon^{96}Zr$	N
Carbonaceous chondrites (CC):							
Orgueil (1)	BM 1920, 328	CI1	0.552	−0.15 ± 0.16	0.05 ± 0.15	0.53 ± 0.34	1
Orgueil (2)	MNHN 234	CI1	1.314	−0.16 ± 0.18	−0.10 ± 0.15	0.15 ± 0.28	2
Orgueil mean				−0.15 ± 0.12	−0.03 ± 0.10	0.30 ± 0.22	
Elephant Moraine	EET 92159	CR2	1.080	−0.15 ± 0.15	−0.27 ± 0.17	0.72 ± 0.71	1
Renazzo	MNHN 38045	CR2	0.208	−0.17 ± 0.15	−0.06 ± 0.15	1.33 ± 0.45	2
CR mean				−0.16 ± 0.11	−0.15 ± 0.11	1.16 ± 0.38	
Cold Bokkeveld	BM 13989	CM2	1.260	−0.07 ± 0.26	−0.20 ± 0.21	1.18 ± 0.63	1
Murray	USNM 1769 (#3)	CM2	1.530	−0.05 ± 0.15	0.12 ± 0.15	0.58 ± 0.29	2
Murchison (1)[†]	USNM 5453	CM2	–	−0.27 ± 0.15	−0.11 ± 0.15	0.19 ± 0.36	1
Murchison (2)[†]	[a,b]	CM2	–	0.02 ± 0.06	0.02 ± 0.06	0.86 ± 0.18	6
Murchison mean		CM2		−0.02 ± 0.06	0.00 ± 0.06	0.73 ± 0.16	
CM mean				−0.03 ± 0.05	0.00 ± 0.05	0.72 ± 0.14	
Allende (1)	[c]	CV3 (Ox)	–	0.06 ± 0.15	−0.02 ± 0.15	1.01 ± 0.27	2
Allende (2)	USNM 3529	CV3 (Ox)	0.600	0.07 ± 0.15	−0.06 ± 0.15	1.39 ± 0.26	1
Allende mean				0.07 ± 0.11	−0.04 ± 0.11	1.21 ± 0.19	
Grosnaja	BM 35217	CV3 (Ox)	1.040	−0.18 ± 0.30	−0.08 ± 0.15	1.01 ± 0.40	1
CV mean				0.04 ± 0.10	−0.05 ± 0.09	1.17 ± 0.17	
Colony	BM 1984 M4	CO3	1.480	−0.02 ± 0.15	−0.05 ± 0.15	0.86 ± 0.25	3
Dar al Gani 137[†]	[a]	CO3	–	−0.05 ± 0.15	0.03 ± 0.15	0.51 ± 0.28	1
CO mean				−0.04 ± 0.11	−0.01 ± 0.11	0.70 ± 0.19	
Dar al Gani 275[†]	[a]	CK4/5	–	−0.01 ± 0.15	0.00 ± 0.15	0.45 ± 0.25	3
Bencubbin	USNM 5717	CB_a	1.600	−0.19 ± 0.15	−0.08 ± 0.15	0.96 ± 0.25	3
Ordinary chondrites (OC):							
Saint-Séverin	MNHN	LL6	1.220	−0.16 ± 0.15	−0.15 ± 0.15	0.34 ± 0.25	3
Forest Vale	–	H4	0.500	−0.16 ± 0.15	−0.07 ± 0.15	0.74 ± 0.25	3
Ste. Marguerite	[d]	H4	–	−0.19 ± 0.15	−0.21 ± 0.15	0.98 ± 0.44	1
Richardton	–	H5	1.020	−0.19 ± 0.15	−0.29 ± 0.15	0.32 ± 0.25	3
OC mean				−0.18 ± 0.08	−0.18 ± 0.08	0.52 ± 0.14	
Enstatite chondrites (EC):							
Abee	USNM 2096	EH4	1.770	−0.09 ± 0.15	−0.20 ± 0.15	−0.25 ± 0.38	2
Indarch	ME 1404 #59	EH4	2.150	0.01 ± 0.26	−0.07 ± 0.15	0.22 ± 0.30	2
EC mean				−0.07 ± 0.13	−0.14 ± 0.11	0.04 ± 0.24	
Eucrites (Euc):							
Pasamonte	USNM 897	Euc-P	0.057	0.02 ± 0.08	−0.07 ± 0.04	0.27 ± 0.11	7
Sioux County	BM 1959	Euc-M	0.050	−0.13 ± 0.06	−0.07 ± 0.04	0.41 ± 0.13	8
Juvinas	#40I(40G)	Euc-M	0.065	−0.09 ± 0.09	−0.06 ± 0.10	0.43 ± 0.18	5
Bouvante	(PE) 3223 MS	Euc-M	0.052	−0.14 ± 0.15	−0.19 ± 0.15	0.50 ± 0.25	4
Bereba	(PE) 1297C MS	Euc-M	0.059	−0.15 ± 0.15	−0.10 ± 0.15	0.73 ± 0.25	4
Euc mean				−0.09 ± 0.04	−0.07 ± 0.03	0.39 ± 0.07	
Mineral separates:							
Chondrules	Allende	CV3	0.111	−0.08 ± 0.37	−0.11 ± 0.20	1.24 ± 0.45	1
Renazzo	Metal-rich wr	CR2	–	0.01 ± 0.15	−0.02 ± 0.15	2.42 ± 0.32	1
Renazzo	Fusion crust (melt)	CR2	0.098	−0.06 ± 0.15	−0.02 ± 0.15	0.33 ± 0.25	2
Forest Vale	Non-magnetic	H4	–	−0.25 ± 0.15	−0.22 ± 0.15	0.63 ± 0.44	1
Hvittis	Non-magnetic	EL6	–	−0.27 ± 0.15	−0.23 ± 0.15	0.56 ± 0.34	4

For samples measured $\leqslant 4$ times, the weighted mean is shown, with the reproducibility (standard deviation, 2σ) of the terrestrial rock standards. For repeat measurements ($n > 4$) of the same sample digest, and independent digests of the same sample (e.g. Orgueil, Allende and Murchison), the weighted mean and its associated uncertainty (2σ) are given. Numbers in parentheses denote digest number. Sample information available from: [a] Sprung et al. (2010), [b] Akram et al. (2013), [c] Schönbächler et al. (2003), [d] Lee and Halliday (2000).

[†] Akram et al. (2013). Murchison (1) digested in microwave.

[‡] Total sample mass powdered from which an aliquot was consumed for digestion and MC–ICPMS analyses.

nucleosynthetic anomalies, it is important to compare the meteorite data to the terrestrial average defined by the terrestrial samples (=composition of the Earth) and not the synthetic Alfa Aesar solution, which yield slightly different Zr isotope compositions. The latter were potentially generated during the production of the synthetic solution.

3.2.2. Enstatite chondrites

The enstatite chondrites are the only meteorites analysed in this study with average $\varepsilon^{91}Zr$ (-0.07 ± 0.13), $\varepsilon^{92}Zr$ (-0.14 ± 0.11) and $\varepsilon^{96}Zr$ (0.04 ± 0.24) values identical to terrestrial rocks. This observation implies that the Earth and enstatite chondrites formed from precursor materials with identical isotopic compositions, as previously suggested based on other isotope systems including O (Clayton, 1993; Wiechert et al., 2001), Cr (Trinquier et al., 2007) and Ni (Regelous et al., 2008).

3.2.3. Ordinary chondrites and eucrites

These two groups yield similar weighted averages of $\varepsilon^{96}Zr = 0.52 \pm 0.14$, and 0.39 ± 0.07, respectively (Table 3). Individual sample measurements show unresolved but consistently more negative $\varepsilon^{91}Zr$ and $\varepsilon^{92}Zr$ values for ordinary chondrites (OC) and less expressed for eucrites (Euc) compared to the terrestrial samples, yielding group averages of $\varepsilon^{91}Zr_{OC} = -0.18 \pm 0.08$, $\varepsilon^{92}Zr_{OC} = -0.18 \pm 0.08$, $\varepsilon^{91}Zr_{Euc} = -0.09 \pm 0.04$ and $\varepsilon^{92}Zr_{Euc} = -0.07 \pm 0.03$.

In summary, the $\varepsilon^{91}Zr$ and $\varepsilon^{92}Zr$ values for individual meteorites are identical to the terrestrial Zr isotope composition (Table 3). Considering the Zr isotope compositions of the group means (weighted average and its associated uncertainty) based on independent analyses, however, reveals potential negative trends in $\varepsilon^{91}Zr$ and $\varepsilon^{92}Zr$ – in addition to the well–resolved positive $\varepsilon^{96}Zr$ (Table 3). Interestingly, in the $\varepsilon^{96}Zr$–$\varepsilon^{91}Zr$ diagram (Fig. 4), the whole-rock data of CI, enstatite and ordinary chondrites as well as eucrites and terrestrial samples (a natural grouping of meteorites suggested by similar Ti and Cr isotope systematics, Trinquier et al., 2009) define a tentative best–fit line (WR) with a slope of -0.144 ± 0.040, and an intercept -0.061 ± 0.011 (95% confidence level, C.L.). This hints that the ^{96}Zr excesses (<1.4 ε) may be correlated with smaller variations in ^{91}Zr. The $\varepsilon^{92}Zr$ values show a similar correlation, but with more scatter. Notably, most carbonaceous chondrites fall to the right (i.e. positive $\varepsilon^{96}Zr$ side) of the WR best–fit line (Fig. 4). This is further explored in Section 4.2.1.

3.3. Components of meteorites

3.3.1. Allende chondrules and CAIs

The Allende chondrule separate (aggregate of many hand-picked chondrules) yield terrestrial $\varepsilon^{91}Zr$ and $\varepsilon^{92}Zr$ values, but a positive $\varepsilon^{96}Zr$ (1.24 ± 0.45, Table 3). Two distinct Zr isotope signatures are reported for Allende CAIs in Akram et al. (2013): the majority (6 out of 8 CAIs) possess similar enrichments ($\varepsilon^{96}Zr = 1.90 \pm 0.09$), which for the purpose of this study, are referred to as *high-$\varepsilon^{96}Zr$* CAIs. Two refractory inclusions CAI_NV_3 and CAI_PS_4 are characterised by resolvable, lower $\varepsilon^{96}Zr$ and define a minor subclass (2 out of 8 CAIs) – referred to here as *low-$\varepsilon^{96}Zr$* CAIs – with a weighted average $\varepsilon^{96}Zr = 0.86 \pm 0.15$. The distinction between these two groups of CAIs is also supported by Hf and Ti isotope data (Akram et al., 2013; Williams et al., 2014). However, the two groups do not possess distinct petrographic features.

3.3.2. Renazzo separates

A metal–rich whole-rock fraction of Renazzo (CR), that yielded an $\varepsilon^{96}Zr$ of 2.0 ± 1.4 in a previous study (Schönbächler et al., 2003) was reanalysed. The excess was refined to an $\varepsilon^{96}Zr$ value of 2.42 ± 0.32 (Table 3), whereas the $\varepsilon^{91}Zr$ and $\varepsilon^{92}Zr$ values still agree with the terrestrial values. Thus, its isotopic composition is distinctly different to that of whole-rock Renazzo ($\varepsilon^{96}Zr = 1.33 \pm 0.45$). This is also correct for the Zr isotope composition of the fusion crust dominated separate of Renazzo ($\varepsilon^{96}Zr = 0.33 \pm 0.25$), which yields a lower $\varepsilon^{96}Zr$ than the whole-rock sample.

3.3.3. Ordinary and enstatite chondrite separates

The *non–magnetic* fractions of the ordinary chondrite Forest Vale (H4) and enstatite chondrite Hvittis (EL6) possess similar, positive $\varepsilon^{96}Zr$ values (~0.6) associated with possible negative $\varepsilon^{91}Zr$ and $\varepsilon^{92}Zr$ (Table 3). For Forest Vale, both the *non–magnetic* and *whole-rock* fractions yield identical Zr isotope compositions within uncertainties. In contrast, the Hvittis *non–magnetic* fraction displays a positive $\varepsilon^{96}Zr$ (0.56 ± 0.34) relative to the *whole-rock* average of enstatite chondrites ($\varepsilon^{96}Zr = 0.04 \pm 0.24$) defined by Abee and Indarch (no whole-rock data for Hvittis are available).

In summary, the Zr isotope compositions of the whole-rock samples of eucrites and carbonaceous chondrites are characterised by $\varepsilon^{91}Zr$ and $\varepsilon^{92}Zr$ values that are identical to those of the Earth. (Table 3). All ordinary chondrites consistently tend towards more negative, but not resolved $\varepsilon^{91}Zr$ values (Table 3). However, potential variations are indicated if the group means and the uncertainties of the weighted average are considered. The data for the non–magnetic fractions also hint at potential $\varepsilon^{91}Zr$ and $\varepsilon^{92}Zr$ variations (see discussion later in Section 4.2.1). For $\varepsilon^{96}Zr$, all samples yield varying degrees of excesses relative to the Earth, with the exception of the enstatite chondrites (Fig. 2; Table 3). Alternative normalization schemes utilising other isotope ratios than $^{94}Zr/^{90}Zr$ (i.e. $^{91}Zr/^{90}Zr$, $^{92}Zr/^{90}Zr$ and $^{94}Zr/^{91}Zr$) were also tested and the results show that the ^{96}Zr excesses are independent of the normalization scheme and hence, are truly located in ^{96}Zr.

4. DISCUSSION

4.1. Carrier phases of anomalous Zr

4.1.1. Refractory inclusions as primary carriers of ^{96}Zr heterogeneities in carbonaceous chondrites

Carbonaceous chondrites contain different amounts of CAIs and this raises the question of whether CAIs are the carriers of the anomalous ^{96}Zr in these samples. This is addressed here using mass balance considerations. Two different two–component mixing models are evaluated: the addition of CAIs to (a) CI and (b) bulk silicate Earth (BSE) material. The Zr isotope composition of a mixture (ε_{mix}, in epsilon) of n components with respective Zr isotopic compositions ε_i is given by:

$$\varepsilon_{mix} = \frac{\sum_{i=1}^{n} C_i w_i \varepsilon_i}{\sum_{i=1}^{n} C_i w_i} \quad (1)$$

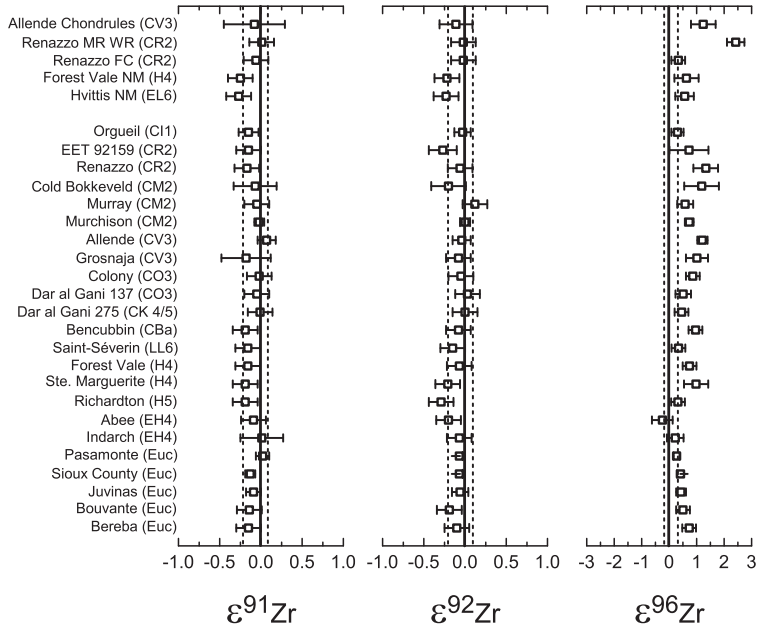

Fig. 2. Zirconium isotope compositions of whole-rock samples and mineral separates. Dashed lines indicate the 2σ standard deviation derived from 73 analyses of the terrestrial rock standards. See Table 2 for sample information and uncertainties. MR WR: metal-rich whole-rock, FC: fusion crust, NM: non-magnetic fraction. Measurements (Murchison, Dar al Gani 137, Dar al Gani 275) from previous studies are highlighted in Table 2.

for the Zr elemental concentrations (C_i) and the mass fractions (w_i) of each component (i), summing over all components $i = 1...n$ (Albarède, 1996). As a first order approximation, we assume that all CAIs possess identical Zr concentrations (~88 ppm Zr; Mason and Taylor, 1982) and ε^{96}Zr enrichments defined by the majority of Allende CAIs: the *high-*ε^{96}*Zr* CAIs ($\varepsilon^{96}Zr = 1.90 \pm 0.09$; Akram et al., 2013). For simplicity, the isotopic compositions of *low-*ε^{96}*Zr* CAIs are neglected in the mass balance calculations, because they only represent approximately ¼ of all Allende CAIs (Akram et al., 2013). Our calculations show, however, that the exclusion of the *low-*ε^{96}*Zr* CAIs does not affect the mass balance calculations significantly (<0.05ε for ^{96}Zr/^{90}Zr). The ε^{96}Zr data of Orgueil and the terrestrial rock standards (Tables 2 and 3) are used as a proxy for the Zr isotope compositions of the CI chondrites (3.96 ppm Zr; Lodders et al., 2009) and BSE (10.5 ppm Zr; McDonough, 2001), respectively. The meteorites are grouped into their classes (CV, CM, CO, CK, CR, CB, CI) and within the same class they are assumed to possess identical Zr isotope compositions. Consequently, the weighted average of each class (Table 3) is compared to the mixing model predictions. The data and mass balance predictions (Eq. (1)) show the best agreement for the CAI – CI chondrite mixing model, and can account for the positive ε^{96}Zr of the CV, CM, CO, and CK groups (Fig. 3), within the analytical uncertainties. Mass balance calculations based on CAI–BSE mixing yield a similar isotope anomaly pattern (CV > CM ≈ CO > CK > CI), but underestimate the overall magnitude of the positive ε^{96}Zr values. Thus, the positive ε^{96}Zr of most carbonaceous chondrites are accounted for by the heterogeneous distribution of CAIs within the accretion region of the carbonaceous

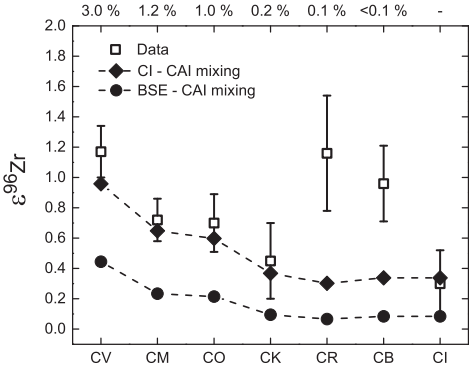

Fig. 3. Mass-balance predictions for (i) CI Chondrite – CAI and (ii) bulk silicate Earth – CAI mixing. Modal CAI abundances Hezel et al. (2008) for different carbonaceous chondrite subgroups are indicated above.

chondrites (between 2.5 and 3.5 AU). Such a heterogeneous distribution is supported by the varying abundances of CAIs in different meteorite classes (Hezel et al., 2008) and is also mirrored by evidence from Ti (Leya et al., 2008) and Sr (Moynier et al., 2010; Hans et al., 2013) isotope variations in carbonaceous chondrites.

Both two–component mixing models (CI and BSE), however, fail to reproduce the significant positive ε^{96}Zr (~1ε) of CB and CR chondrites, which are almost devoid of CAIs. This indicates that at least one additional carrier phase of anomalous ^{96}Zr must be either present or was preferentially lost in these meteorites.

Refractory inclusions may also have been important for the Zr isotope composition of Allende (CV3) chondrules.

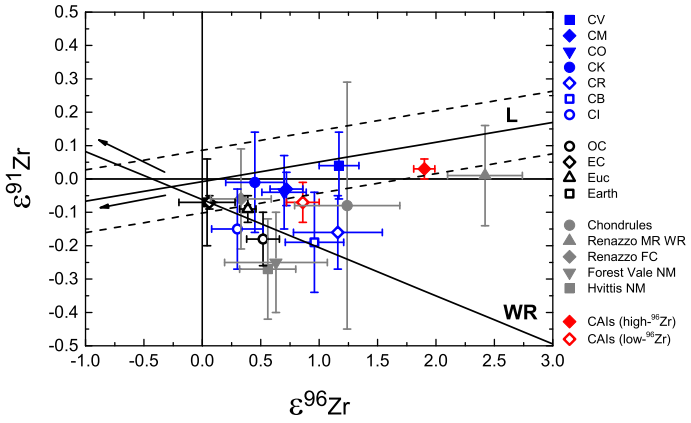

Fig. 4. The $\varepsilon^{96}Zr$ and $\varepsilon^{91}Zr$ data for whole-rock samples and mineral separates. WR denotes the whole-rock best–fit line tentatively defined by a subset of the samples (see text, Section 3.2). L represents the leachate best–fit line with the 2σ uncertainty band (black dashed lines) from Schönbächler et al. (2005). The data are not corrected for the small offset ($\varepsilon^{91}Zr = -0.07$) between terrestrial samples and the Alfa Aesar standard solution, affecting the data of this study, but not necessarily that of Schönbächler et al. (2005). The directions of the corresponding s-process end member for lines WR and L are denoted with an arrow. E: Earth, Euc: eucrites, OC: ordinary chondrites, EC: enstatite chondrites, MR WR: metal-rich whole-rock, FC: fusion crust, NM: non-magnetic.

Chondrules experienced multiple episodes of heating and cooling (Jones et al., 2000) during which they potentially sampled relic CAI material (Krot and Keil, 2002; Krot et al., 2002, 2004). It is therefore possible that the chondrules inherited their positive $\varepsilon^{96}Zr$ signature ($\varepsilon^{96}Zr = 1.24 \pm 0.45$, averaged over multiple chondrules), or a part of it, from CAIs. Mass balance calculations show that chondrules would need to incorporate approximately 10% CAI material to account for their Zr isotope composition, assuming CI-chondrite starting material for the chondrules. Further investigations are needed to substantiate this idea and to show whether the positive $\varepsilon^{96}Zr$ excesses are uniform within individual chondrules.

The Zr isotope composition of Allende matrix was estimated using a three-component model (bulk Allende = matrix + chondrules + CAIs) based on Eq. (1). The model calculation utilized: (i) the Zr isotope composition of bulk Allende, chondrules and CAIs (Tables 2 and 3), (ii) the Zr concentration of CAIs (Mason and Taylor, 1982), bulk Allende (Schönbächler et al., 2005) and Allende chondrules. Since the Zr abundances of chondrules were not accurately determined, the chondrule concentrations are estimated to be twice that of bulk Allende, based on Ti concentrations in the same samples. Furthermore, it was assumed that bulk Allende contains 3% CAIs (Hezel et al., 2008), 45% chondrules (Scott and Krot, 2007), with the remaining material (52%) as matrix. The calculations yield an Allende matrix with an $\varepsilon^{96}Zr$ of 0.36 ± 0.70 (2σ uncertainty). This value is comparable to the Zr isotope composition of CI chondrites ($\varepsilon^{96}Zr = 0.30 \pm 0.22$). This similarity of Allende matrix with CI chondrites supports the idea that the matrices of different carbonaceous chondrites possess identical (CI) isotopic compositions (Alexander, 2005).

4.1.2. Additional carriers of anomalous Zirconium

In the previous section, it was shown that CAIs cannot be the only carriers of anomalous Zr in chondrites (Fig. 3). In the following, evidence is presented for other carrier phases of anomalous Zr.

4.1.2.1. Metal-rich and labile carriers in Renazzo (CR2).

The data of the metal-rich fraction of Renazzo ($\varepsilon^{96}Zr = 2.42 \pm 0.32$) suggest the presence of a ^{96}Zr-rich carrier, which is different to the ^{96}Zr carrier phase in CAIs, because the latter is not related to metal. The similar Zr isotope compositions of both the metal–rich Renazzo fraction and CAIs (high-96, Fig. 4), however, hint at a similar nucleosynthetic origin for both components. Potentially this nucleosynthetic signature was originally located in the same phase, but was subsequently altered during CAI formation and/or in Renazzo due to secondary processes.

The low $\varepsilon^{96}Zr$ value of the Renazzo fusion crust ($\varepsilon^{96}Zr = 0.33 \pm 0.25$) is unlikely due to terrestrial contamination, because at least twice as much terrestrial Zr must be added to the starting material (i.e. Renazzo) to sufficiently lower the $\varepsilon^{96}Zr$ value based on mass balance considerations. However, the Zr concentration of the fusion crust sample was not substantially enhanced relative to bulk-rock Renazzo, which excludes a strong terrestrial contamination. Fusion crust represents quenched melts, which experienced high temperatures during the travel of the meteoroid through the Earth's atmosphere. It is thus conceivable that more labile ^{96}Zr bearing phases were removed by vaporisation. If this idea is correct, this provides evidence for a thermally labile ^{96}Zr carrier in Renazzo. Potential candidates are, e.g., metal or organic matter (Le Guillou et al., 2014) that was burned off during the travel through the atmosphere. This does not necessarily imply that organic matter carries the anomalous ^{96}Zr itself, but that this actual carrier is associated with organic matter that is destroyed during the entry of the meteoroid.

4.1.2.2. Non-magnetic fractions of Hvittis (EC, EL6) and Forest Vale (OC, H4).

The non-magnetic fraction of the enstatite chondrite Hvittis reveals anomalies in $\varepsilon^{96}Zr$, with potential negative trends in $\varepsilon^{91}Zr$ and $\varepsilon^{92}Zr$ relative to the Earth and whole-rock enstatite chondrites (Table 3). This implies that a component within the non-magnetic fraction carries the anomalous Zr. This carrier may be silicates,

because they are the major component of the non-magnetic fraction and contain significant amounts of refractory lithophile elements like Zr. In contrast to enstatite chondrites, the ordinary chondrite Forest Vale yields identical Zr isotope compositions for bulk-rock and its non-magnetic fraction within the analytical uncertainty. This composition is distinct from terrestrial rocks, but identical to the non-magnetic fraction of Hvittis. This implies that the anomalous Zr from the Forest Vale non-magnetic fraction (silicates) dominates the bulk Zr budget of ordinary chondrites, while it is less pronounced in enstatite chondrites. In line with this observation, in the three isotope diagram (Fig. 4), the composition of the non-magnetic fraction of Forest Vale, overlaps with the WR best–fit line (Fig. 4) and possesses more extreme Zr isotope compositions than the Earth and bulk enstatite chondrites. The non-magnetic fraction of Hvittis falls slightly off the line, but still falls within the error envelop of the line. Hence, taken at face value, the heterogeneous distribution of these specific silicates identified in the non-magnetic fraction likely caused the WR correlation and they contributed a greater proportion to ordinary chondrites than the Earth and enstatite chondrites. This conclusion is in agreement with the increased thermal destruction of silicates within the solar nebula as a function of distance to the sun (further discussed in Section 4.2.4).

Collectively, the data provides evidence for at least three distinct carrier phases (CAIs and potentially a metal/organic related carrier and silicates) of anomalous Zr, which are present in different proportions in various solar system materials and carry at least two different nucleosynthetic fingerprints.

4.1.3. A three-component mixture for whole-rock Zr isotope variations

Overall a three-component mixture is indicated based on grouped Zr isotope measurements when the data are shown in a three-isotope diagram (Fig. 4). The ε^{96}Zr values are tentatively correlated with possible variations in ε^{91}Zr and ε^{92}Zr (discussed in Section 4.2). The offset for CV, CM, CO and CK chondrites can be attributed to the addition of CAIs to either (i) CI material (Figs. 3 and 4) or (ii) to solar system material that spreads along the WR correlation. The metal/organic carrier with a similar isotopic composition as *high-ε^{96}Zr* CAIs explains the CR and CB data, while their CAI content ($\leqslant$0.1%) is too low to account for the offset from the WR line. Summarising, the Zr isotope data of bulk-rock samples can be explained by a three-component mixing, with (i) a high ε^{96}Zr end member (sampled most extensively by CAIs and Renazzo metal-rich whole-rock) and (ii) a silicate end member with anomalous Zr, which are admixed to (iii) the remaining solar system material. The mixing between the silicate end member and the remaining solar system material causes the tentative WR correlation (Fig. 4). It is important to note that this three-component model adequately explains the Zr isotope compositions of the meteorites, but does not directly relate to the bulk elemental compositions of these meteorites.

4.2. Nucleosynthetic origin of Zr isotope variations in the inner solar system

This section discusses the nucleosynthetic origin of the Zr isotope variations in the solar system for whole-rock samples (this work) and acid leachates (Schönbächler et al., 2005). Since Zr is dominantly synthesised by the *main s-process* in LM and IM AGB stars (e.g., Travaglio et al., 2004), comparisons are provided with other mainly s-process elements such as the neighbouring elements Mo, and to some extent Ru, that are in a similar mass range as Zr. This section identifies parallels between these isotope data sets, which show a similar trend, and discusses viable mechanisms that are responsible for this isotope variability.

4.2.1. Origin of the whole-rock (WR) Zr isotope correlation

Variable addition (or removal) of material from specific nucleosynthetic sources to (or from) the solar nebula is considered to explain the nucleosynthetic origin of the Zr isotope variations. Nucleosynthesis by the main s–process is evaluated first, because Zr is mainly an s–process element. Our approach follows the formulation derived in Dauphas et al. (2004). This allows us to directly compare stellar isotope yields with ε^{i}Zr ($i = 91, 92, 96$) values of solar system materials. It also accounts for the assumption of a fixed ^{94}Zr/^{90}Zr ratio (=0.3381) for all samples, which is necessary to adequately correct for the instrumental mass bias and achieve high precision isotope data. The model entails that materials produced in a stellar source were admixed in various proportions to solar system materials with $\varepsilon^{i}\mathrm{Zr} = 0$ (terrestrial composition). Any mixture of the two components (e.g., terrestrial and s–process material) must fall on a mixing line, in ε^{96}Zr–ε^{91}Zr space, defined by:

$$\varepsilon^{91}\mathrm{Zr} = \frac{\rho^{91}_{\mathrm{Zr}} - \rho^{94}_{\mathrm{Zr}}\mu^{91}\mathrm{Zr}}{\rho^{96}_{\mathrm{Zr}} - \rho^{94}_{\mathrm{Zr}}\mu^{96}\mathrm{Zr}}\varepsilon^{96}\mathrm{Zr} \quad (2)$$

where

$$\rho^{i}_{\mathrm{Zr}} = \frac{(^{i}\mathrm{Zr}/^{90}\mathrm{Zr})_{s}}{(^{i}\mathrm{Zr}/^{90}\mathrm{Zr})_{t}} - 1 \quad (3)$$

relates the Zr isotope ratios of the terrestrial (t) and s–process (s) end member components, normalized relative to ^{90}Zr. The term

$$\mu^{i}\mathrm{Zr} = \frac{(^{i}\mathrm{Zr} - {}^{90}\mathrm{Zr})}{(^{94}\mathrm{Zr} - {}^{90}\mathrm{Zr})} \quad (4)$$

is proportional to the mass difference between ^{i}Zr and ^{90}Zr, and the masses of isotopes (^{94}Zr and ^{90}Zr) used for the instrumental mass bias correction.

For the s-process end member, new Zr isotope abundances are adopted from updated stellar models. These new models surpass the stellar model presented in Arlandini et al. (1999), which reports the *average* Zr isotope composition of both 1.5 $M_{\odot}$ and 3 $M_{\odot}$ AGB stars with half-solar metallicity. The stellar models considered here are based on Bisterzo et al. (2011a), and build on the model of Arlandini et al. (1999) by incorporating a more extensive nuclear reaction network and improved neutron-capture rates (e.g., ^{i}Zr(n,γ)$^{i+1}$Zr reaction rates). *Individual* stellar

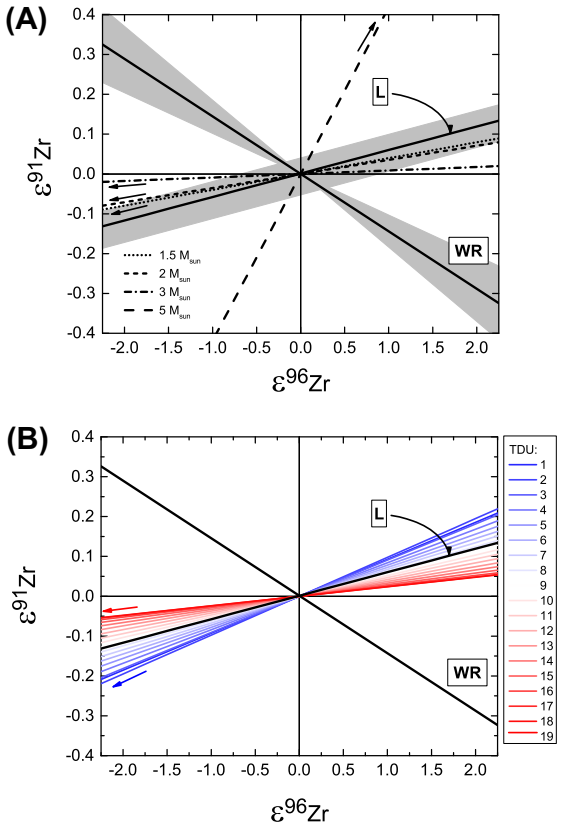

Fig. 5. Mixing lines between different s–process end members and the terrestrial Zr isotope composition. Arrows indicate direction of s-process source. Best–fit lines defined by whole-rock samples, WR (this study, see text) and leachate data, L (Schönbächler et al. (2005)) are also shown. For simplicity, the whole-rock line is corrected for an offset from the origin (-0.06 ± 0.011) and forced though $\varepsilon^{91}Zr = \varepsilon^{96}Zr = 0$, such that Eq. (2) can be used in its current form. This does not affect the interpretation of the data, which is based on gradients. (A) Mixing lines for admixing of material from AGB stars with different initial masses (Bisterzo et al. (2011); this study) with a terrestrial composition. For the whole-rock mixing line, the uncertainties (grey band) are dominated by the uncertainties on the gradient (-0.144 ± 0.040), whereas for the leachate mixing line they are dominated by uncertainties on the intercept (-0.007 ± 0.047; Schönbächler et al. (2005)). (B) Mixing lines for the envelope compositions of a 3 $M_{\odot}$ AGB star during 19 progressive TDUs are illustrated.

yields for AGB stars with different initial masses (1.5, 2, 3 and 5 $M_{\odot}$), metallicities (solar, half-solar) and ^{13}C pocket efficiencies (e.g. see Lugaro et al., 2003; Bisterzo et al., 2011a,b) are explored (Fig. 5A). Massive stars (>8 $M_{\odot}$, weak s-process sites) and low-metallicity stars are neglected, because they produce very little (Raiteri et al., 1993) or no Zr (e.g. Travaglio et al., 2004), respectively. The effects of varying metallicity (solar or half–solar) and ^{13}C pocket efficiencies, for a fixed initial stellar mass, on the resultant Zr isotope compositions were determined and do not affect the compositions significantly. In addition to the models that report final envelope compositions of AGB stars (Arlandini et al., 1999; Bisterzo et al., 2011b) (Fig. 5A), the Zr isotope yields within the stellar envelopes of individual LM and IM stars at *different times* of their AGB phases are also evaluated (Fig. 5B). The temporal evolution of a star along its AGB phase is tracked by the total number of third dredge ups (TDUs) elapsed. Each TDU represents instances where newly synthesized s-process material, during periodic thermal pulses, is dredged up and mixed with the envelope. The C/O ratio of the envelope monotonically increases with each progressive TDU (Fig. 5B), and the envelope becomes more enriched in s-process material. With each TDU, the envelope develops more positive $\varepsilon^{91}Zr$ and $\varepsilon^{96}Zr$ values, which span a wide range of values over the course of the AGB lifetime.

Our model results (Fig. 5A) illustrate that it is not possible to identify a unique s-process source (i.e. AGB star) that is consistent with the solar system WR heterogeneity. However, the models predict a mixing line in $\varepsilon^{96}Zr$–$\varepsilon^{91}Zr$ space, consistent with the whole-rock best fit line (WR), when combining average yields of various AGB stars (LM and IM) (Fig. 5A). This provides evidence that the WR Zr isotope heterogeneity (defined by CI, enstatite and ordinary chondrites, eucrites and the Earth) is due to s-process materials, which originated from multiple LM and IM AGB stars.

4.2.2. Origin of nucleosynthetic Zr isotope variations resolved in leachate experiments

Well-resolved evidence for correlated $\varepsilon^{96}Zr$–$\varepsilon^{91}Zr$ variations in solar system materials originates from stepwise acid-leaching experiments carried out on the carbonaceous chondrites Allende, Murchison and Orgueil (Schönbächler et al., 2005). The leachate data define a best–fit line, *L*, in $\varepsilon^{96}Zr$–$\varepsilon^{91}Zr$ space characterized by a slope 0.059 ± 0.003 and an intercept -0.007 ± 0.047, with an s-process signature attributed to phases with $\varepsilon^{96}Zr < 0$ (and $\varepsilon^{91}Zr$, $\varepsilon^{92}Zr < 0$) and a complimentary r-process signature for phases with $\varepsilon^{96}Zr > 0$ (Figs. 4 and 5). The final leaching steps, containing the refractory presolar SiC grains, reveal an isotopic composition consistent with the admixture of these grains (Nicolussi et al., 1997; Davis et al., 1999a, Schönbächler et al., 2005). The leachate line is almost orthogonal to the tentative whole-rock correlation, posited by the new data and models. Therefore, the leachate and whole-rock data require distinct s-process end members with $\varepsilon^{91}Zr < 0$ and $\varepsilon^{91}Zr > 0$, respectively.

The mixing lines based on the newly determined s–process yields succeed in reproducing the leachate correlation for stars with low initial masses (1.5 $M_{\odot}$, 2 $M_{\odot}$ and 3 $M_{\odot}$) (Fig. 5b). Models utilizing higher initial stellar masses (e.g. 5 $M_{\odot}$, Fig. 5a) fail to reproduce the leachate best-fit line because they incorporate a high neutron–density burst from the $^{22}Ne(\alpha,n)^{25}Mg$ reaction, leading to envelope compositions with positive $\varepsilon^{91}Zr$ and $\varepsilon^{96}Zr$.

These observations have several implications. *Firstly*, the correlation of the C/O ratio with $\varepsilon^{91}Zr$ values implies that the s-process Zr with lower $\varepsilon^{91}Zr$ should largely reside within oxides because these phases condense in an environment with low C/O. Carbides should have higher $\varepsilon^{91}Zr$ because they condense at C/O > 1 (Fig. 5B). The results from the Zr leachate experiments indicate that the leachate correlation (L) is largely caused by s-process Zr that is located in mainstream SiC grains and an additional

unidentified carrier phase, potentially silicates or an easily leachable phase with an r-process signature (Schönbächler et al., 2005). Later leachate studies on carbonaceous chondrites using Os isotopes support this conclusion (Yokoyama et al., 2007; Reisberg et al., 2009). Since the leachate data is consistent with SiC grains and silicates, this is in good agreement with our model results, which places the leachate best fit line in the transition zone between carbides and oxides.

However, these results need to be considered with caution because the predicted s-process Zr isotope abundances have model uncertainties. For example, one aspect that is not considered with regards to the C/O ratio of the AGB star is cool bottom burning (e.g. see Zinner et al., 2005), which reduces the amount of ^{12}C and produces a larger number of TDUs with $C/O > 1$. Moreover, the $^{95}Zr(n,\gamma)^{96}Zr$ Maxwellian–averaged cross section (MACS) is the largest source of uncertainty for ^{96}Zr yields, owing to the instability of ^{95}Zr. Current theoretical estimates of this value vary from 24 mb (Goriely, 2002) to 140 mb (Shibata et al., 2002; Chadwick et al., 2006), with models presented in this study adopting a value of 50 mb (based on semi-empirical estimates, Toukan and Käppeler, 1990). Hence, the current value for the $^{95}Zr(n,\gamma)^{96}Zr$ MACS can be lowered by a factor of two and still remain within the overall range of the quoted cross-sections. Revised calculations with lower values yield less negative $\varepsilon^{91}Zr$ values for the corresponding C/O ratios, which would shift the leachate best-fit line more towards the SiC field. A similar outcome is achieved when the calculations are repeated for a reduced $^{22}Ne(\alpha,n)^{25}Mg$ reaction rate (Jaeger et al., 2001). In summary, combining the evidence from the leachate data and nucleosynthetic models suggests that carbonaceous chondrites received variable contributions of s–process matter in the form of, e.g., silicates and oxides that were dredged up early on, in addition to SiC grains that formed during later TDUs. These phases are partially resolved during leaching experiments.

Secondly, an important outcome of this study is that nucleosynthetic trends discovered in leaching experiments of carbonaceous chondrites are not necessarily indicative of the bulk-rock isotope heterogeneity. Our data suggest that bulk-rock samples and leachates may not define the same isotopic trends (Fig. 4). In agreement with our conclusion, correlated trends for W and Mo isotopes were identified for leach experiments, but not for bulk-rock samples (Burkhardt et al., 2012). Leachate experiments have been widely applied (e.g., Rotaru et al., 1992; Dauphas et al., 2002b; Schönbächler et al., 2005; Yokoyama et al., 2007) to identify the nucleosynthetic components from which our solar system was formed. However, these resolved nucleosynthetic components may not bare a direct connection to the bulk-rock isotope heterogeneities observed in solar system materials. Hence, they are homogeneously distributed in the solar system. Components identified by Zr leaching experiments sample a very specific and restricted range of nucleosynthetic sources, limited to LM AGB stars. This stands in contrast to the tentative bulk-rock heterogeneity outlined in this study, which is best explained by mixing of material from multiple AGB stars (LM and IM), therefore being more representative of the average s-process Zr composition our solar system.

Thirdly, the multitude of different s-process end member compositions unraveled for Zr also testify to the non-applicability of the r-residual method for Zr, since it is not evident what the complementary r-process signature is for Zr based on a wealth of different s-process mixing lines. Consequently, it is not possible to posit, for Zr at least, that an r-excess signature is equivalent to an s-deficit signature. Moreover, the non-applicability of the r-residual method for Zr has also been pointed out by previous work (Bisterzo et al., 2011), based on the fact that nucleosynthetic theory allows for various processes (in addition to the r- and p-process) to produce the non-s-process isotopes in the mass range below Ba isotopes.

4.2.3. Correlations between the Zr and Mo isotope systems

The ^{96}Zr variations (Table 3, Fig. 2) correlate with those of Mo isotopes for (i) whole-rock samples of chondrites and the Earth (Fig. 6) and (ii) – with more scatter – acid leachates of the carbonaceous chondrites Orgueil and Murchison (Burkhardt et al., 2011, 2012; Dauphas et al., 2002b). In addition, a correlation between Mo and Ru isotopes was proposed (Dauphas et al., 2004; Chen et al., 2010) and this entails that Ru isotope variations are also correlated with Zr isotopes. However, due to the very limited Ru data currently available, the discussion here is restricted to Mo and Zr. Their isotope systematics exhibit two major differences, despite the refractory nature and similar masses of Zr and Mo. Firstly, the Mo isotope data for both whole-rock meteorites and acid leachates of carbonaceous chondrites fall on *the same s-process* mixing line in a Mo three isotope diagram (Burkhardt et al., 2012). This stands in contrast to the interpretation of the Zr data in light of the new models (Figs. 2 and 4) and warrants an explanation. The updated stellar model (Section 4.2.1) was also evaluated for Mo isotopes. Molybdenum and Zr isotopes differ because of the significantly lower neutron–capture cross sections of Zr isotopes and the neutron–capture pathway of Zr, which is more sensitive to branching's

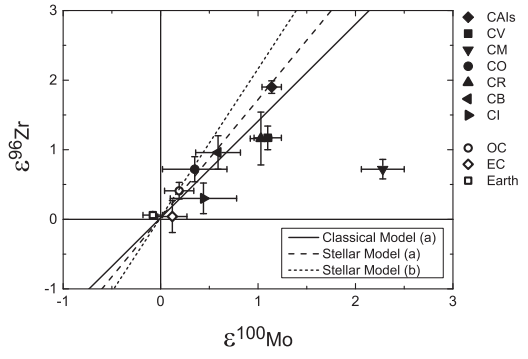

Fig. 6. The Zr and Mo isotope compositions for the Earth, carbonaceous, ordinary and enstatite chondrites, and high $\varepsilon^{96}Zr$ CAIs. The Mo isotope data are from Burkhardt et al. (2011). Also shown are the mixing lines computed for the addition of s-process Zr and Mo predicted from the classical and stellar AGB models: ((a) Arlandini et al. (1999), (b) Bisterzo et al. (2011)) to a terrestrial composition.

(at ^{85}Kr, ^{86}Rb, ^{95}Zr, Lugaro et al., 2003). The resulting calculations yield very limited variation for the Mo isotope compositions in the envelope of LM stars in their AGB phases, resulting in very few distinct s-process end members (and thus a smaller spread in mixing lines). Furthermore, LM AGB stars can account for the bulk (87%) of the s-process Mo in the solar system (Arlandini et al., 1999; Travaglio et al., 2004). In contrast, Zr receives significant s–process contributions from both LM and IM AGB stars (Travaglio et al., 2004, Fig. 5A) and a star along the AGB track produces a wide range of different Zr isotope abundances (Fig. 5B). This is consistent with the distinct s–process Zr signatures revealed by the whole-rock and leachate data, whereas Mo isotope data do not show this distinction (Burkhardt et al., 2012). It also emphasizes the sensitivity of Zr isotope production factors (in contrast to those of Mo isotopes) to different model parameters, which implies that Zr isotopes are a sensitive tracer to monitor the production of s–process material in (i) stars of different masses ($\leqslant 8\ M_{\odot}$) and (ii) during the evolutionary phases of a particular AGB star. These findings are consistent with earlier work on presolar grains (Nicolussi et al., 1997; Davis et al., 1999a) that demonstrates that a number of AGB stars, with different masses, are required to explain the dispersion in the Zr isotope compositions among single presolar SiC grains (Lugaro et al., 2003).

Another clear difference between Mo and Zr isotope systematics is that the majority of the carbonaceous chondrites reveal a departure from the s–process WR mixing line for Zr isotopes, as a result of the addition of CAIs (this study), whereas no such deviation is postulated for Mo (Burkhardt et al., 2011). Allende CAIs are enriched in neutron-rich isotopes for both Zr (Akram et al., 2013) and Mo (^{100}Mo enrichments in Type B CAIs, Burkhardt et al., 2011). However, the majority of analysed CAIs exhibit less positive Mo isotope anomalies relative to CV chondrites, and the anomaly pattern observed for these CAIs are characteristic of an r-excess (Burkhardt et al., 2011). The addition of CAIs to chondritic material, therefore, affects the Zr isotope composition more than that of Mo and thus influences the Zr whole-rock correlation more. Nevertheless, the ε^{96}Zr and ε^{100}Mo isotope composition of the Earth and bulk meteorites show a good correlation (Fig. 6). There is some scatter, however, particularly as Murchison (and Allende) falls to the right of the correlation line with a large positive ε^{100}Mo. The presence of CAIs can explain the small offset for Allende, whereas this is not the case for Murchison. The Mo and Zr excesses of Murchison increase through incomplete dissolutions of the meteorite (Burkhardt et al., 2012; Akram et al., 2013). However, Akram et al. (2013) could show that the Zr effect was generated through incomplete dissolution of SiC grain, while Burkhardt et al. (2012) showed that another carrier phase was needed for Mo. This demonstrates that the overall budget of anomalous Zr and Mo is distributed differently within the various carrier phases, although both elements occur in SiC grains. This is not surprising because Zr is a strictly lithophile element in contrast to Mo. For example, the Mo isotope variations in Murchison may be related to a refractory metal carrier largely devoid of Zr. It is possible that the Mo-Zr separation was already a feature of the presolar grains. On the other hand, a redistribution of Zr and Mo from a single carrier into multiple carriers could also have occurred in the solar nebula and/or in the meteorite parent body, because all meteorites sampled material that was processed in the solar nebula and experienced parent body processing. The reprocessing, however, must have been a local phenomenon to preserve the overall bulk-rock Zr-Mo correlation. For example, carbonaceous chondrites experienced different degrees of aqueous alteration. Aqueous alteration has affected presolar phases such a silicates, which carry Zr and Mo. This alteration did not lead to a significant decoupling of Mo and Zr isotopes. Such a decoupling, however, could be expected because Zr is an immobile element, while Mo is sensitive to oxidation and therefore more likely to interact with and be transported by the fluid. Since a decoupling is not observed, this requires that the alteration affected the Zr and Mo isotopes on a local scale only, which is smaller than probed by the data. This observation also indicates that the overall bulk heterogeneities were established before parent body alteration took place as discussed in Section 4.2.4.

In summary, the overall correlation between the two isotopic systems suggests that Zr and Mo isotopes in the solar system mainly originate from similar nucleosynthetic sources. The Mo isotope variations were attributed to different accretionary regions of the solar system that contained variable amounts of s–process material, most likely from LM AGB stars (Dauphas et al., 2004; Burkhardt et al., 2011). The Zr isotope data in combination with the new s-process models require the input of both LM and IM stars, and thus envisage the heterogenous distribution of an s-process component that consists of material from multiple sources. This is not a contradiction because Mo isotopes are not sensitive to this distinction. Nebular processes are considered as likely mechanisms for the distribution of this s-process material, having excluded a widespread form of parent body processing (aqueous alteration).

4.2.4. Dust processing and the heterogeneous distribution of s–process material

4.2.4.1. Injection by a single stellar source. The Zr isotope data support a heterogeneous distribution of different s–process phases (e.g., SiC, oxides and silicates) from *multiple* stellar sources (LM and IM AGB stars). Interestingly, one heterogeneously distributed s-process component is identical to the average solar system s–process composition obtained from models and astronomical observations (Arlandini et al., 1999; Lugaro et al., 2003; Bisterzo et al., 2011). The variable distribution of such a unique s-process mixture cannot be achieved with a *single* event, such as a nearby supernova event (e.g. Lee et al., 1976) or an AGB star (low probability; Kastner and Myers, 1994) that injected nucleosynthetic material into the solar nebula. Moreover, the late injection of material from *multiple* stellar sources appears unlikely since the solar system overall is very well mixed to a first order (e.g. Schönbächler et al., 2003). Hence, a sorting mechanism, within the solar nebula, is required that is able to act on various presolar

carriers from multiple nucleosynthetic sources. This is best achieved, when starting with a well–mixed protosolar molecular cloud. Selective dust sorting then occurs during solar system formation either (i) through the strong stellar winds (e.g. Dauphas et al., 2010) or (ii) through the selective destructions of more thermally more-labile phases caused by the temperature gradients in protoplanetary disk (e.g., Trinquier et al., 2009).

4.2.4.2. Grain-size sorting. The ε^{96}Zr values of bulk meteorites vary proportionately with those of ε^{50}Ti (Schönbächler et al., 2011). The latter in turn correlate with ε^{54}Cr (Trinquier et al., 2009). The Ti isotope data per se are consistent with bulk-rock isotope variations that define a WR correlation line and the offset of specific carbonaceous chondrites from the WR line through CAI addition (Leya et al., 2008; Trinquier et al., 2009; Zhang et al., 2012). The ^{54}Cr variations were attributed to the heterogeneous distribution of nm–sized spinels (Dauphas et al., 2010; Qin et al., 2011) that were sorted by strong stellar winds (Dauphas et al., 2010). However, these spinels display low Ti concentrations and are not the carrier of the ε^{50}Ti excesses (Qin et al., 2011). Therefore, if taken at face value, the ^{96}Zr, ^{50}Ti and ^{54}Cr anomalies must be hosted in different carrier phases. The similar systematics of these anomalies suggest that the carrier phases of ^{96}Zr and ^{50}Ti reacted to the stellar winds the same way as the ^{54}Cr-rich spinels. Although this cannot be excluded, it appears unlikely and therefore we favour thermal processing as the origin of the heterogeneity at the bulk-rock scale.

4.2.4.3. Thermal processing. Nucleosynthetic anomalies reported to date are restricted to refractory or relatively refractory elements (e.g., Cr (Rotaru et al., 1992; Podosek et al., 1997; Lugmair and Shukolyukov, 2001; Trinquier et al., 2007), Ti (Niemeyer and Lugmair, 1984; Leya et al., 2008; Trinquier et al., 2009; Zhang et al., 2012), Ni (Regelous et al., 2008; Steele et al., 2012), Ca (Simon et al., 2009; Chen et al., 2011), Zr (Akram et al., 2013), Mo (Dauphas et al., 2002a; Chen et al., 2004; Burkhardt et al., 2011), Ru (Chen et al., 2010), Ba (Ranen and Jacobsen, 2006; Carlson et al., 2007)), which further substantiates that a refractory nature of a given element is essential for the preservation of nucleosynthetic anomalies (Clayton et al., 1988). The Earth shows an excess in s–process Zr (and Mo) isotopes relative to meteorites (Figs. 2 and 4), which indicates (i) the addition of s–process material to the Earth or (ii) the *removal* of non-s-process material (i.e. formed in supernovae/novae and other stellar sources) from hotter regions closer to the Sun where the Earth accreted. Thermal processing entails the selective destruction of carrier phases because of their distinct susceptibilities to temperature (Trinquier et al., 2009) and thus requires option (ii). This implies that on average, part of the materials produced in supernovae or other non-AGB stellar environments (r- and p-process sites) are more susceptible to thermal destruction than material from AGB stars (s-process). The difference could be due to grains characterised by smaller sizes and/or the chemical composition of the grains. Since the variations along the WR line may be caused by a silicate carrier (Section 4.1.2), the size of the grains appears the more likely option.

In summary, the Zr isotope variations observed in CI, enstatite and ordinary chondrites, eucrites and the Earth (reflected by the WR best fit line) can be explained by the better resistance to thermal processing of s-process material produced in AGB stars. This led to an enrichment of s-process material in the Earth compared to meteorites that formed further away from the Sun. The isotopic budgets of elements heavier than, and including Ba (e.g. Hf and W; Sprung et al., 2010; Burkhardt et al., 2012) show isotopic homogeneity on the bulk-rock scale and were therefore not affected. This is likely the result of their different nucleosynthetic origin (e.g. see Akram et al., 2013). They are primarily produced by the main r–process, which may not contribute significantly to the lower mass elements.

5. CONCLUSIONS

New high–precision Zr isotope analyses for whole-rock samples of meteorites, mineral separates of Renazzo (CR), Forest Vale (H4) and Hvittis (EL6), and a chondrule separate are presented. The data provide evidence for a wide–range of nucleosynthetic Zr isotope variations at a bulk–rock level for various meteorites and on a local scale within carbonaceous and enstatite chondrites.

The mineral separate data reveal at least three different carrier phases of anomalous Zr, with at least two distinct nucleosynthetic fingerprints. Normal CAIs are divided into *high-*ε^{96}*Zr* (3/4) and *low-*ε^{96}*Zr* (1/4) CAIs based on their different ε^{96}Zr values. This division does not correlate with the petrographic features or the rare earth element based grouping of the CAIs. The majority of CAIs exhibit larger ε^{96}Zr excesses than the *low-*ε^{96}*Zr* CAIs, and on average slightly elevated ε^{91}Zr and ε^{92}Zr values compared to the terrestrial samples (Fig. 4). This is similar to the isotopic signature of the metal-rich and fusion crust fractions of Renazzo. These analyses also provide evidence for thermally labile carrier phases (e.g. *organic compounds, or a phase related to organics and/or metal*). The nucleosynthetic origin of this Zr isotope signature was attributed to CPRs in core-collapse, type II supernovae (Akram et al., 2013). Interestingly, the comparison of the non-magnetic fraction of enstatite chondrites with those of ordinary chondrites and their bulk-rock samples indicate the presence of a non–magnetic carrier (potentially *silicates*) characterized by ε^{96}Zr excesses.

We propose three nucleosynthetic end members to explain all the bulk-rock Zr isotope data. Ordinary, enstatite and CI chondrites, eucrites and terrestrial samples tentatively define a linear correlation (WR) in the Zr three–isotope space. Some carbonaceous chondrites fall off this trend towards the isotopic composition of *high-*ε^{96}*Zr* CAIs, which is consistent with the admixture of various amounts of CAIs in these meteorites. New and updated s–process models are explored and show that a wide range of Zr isotope compositions, and correlated Zr isotope patterns, are produced over the evolutionary timescale of a single star in its AGB phase, and by AGB stars with different initial stellar masses. The posited Zr bulk-rock correlation

(WR) is consistent with the heterogeneous distribution of average solar system s–process material, which represents a mixture of material produced in many stars (LM and IM AGB stars). Parent body processes, such as aqueous alteration are unlikely to have caused this large-scale heterogeneity, and this points to nebular processes. In the context of thermal processing, the data imply that a mixture of non–s-process material was destroyed more readily in the solar nebula through heating and this may be related to the grain size (i.e. more resistant s–process dust due to larger grain sizes). Our mineral separation data indicates that silicates may be the presolar phases responsible for the tentative WR correlation.

In contrast to the interpretation of the bulk–rock results, the Zr isotope leachate data of carbonaceous chondrites (Schönbächler et al., 2005) define a clear correlation in the three-isotope space that is best explained by materials that formed exclusively in LM AGB stars. This different origin provides evidence that leaching experiments do not necessarily resolve the nucleosynthetic components that are distributed heterogeneously at a bulk-rock scale.

The isotopic differences between the Earth and meteorites further substantiate that the analysed meteorites are not the exact building blocks of the Earth. Since the Earth accreted from a mixture of material with different degrees of volatile depletion (Schönbächler et al., 2010) and the Zr isotope composition of the Earth falls at the end of the WR correlation (most enriched in s–process materials), this furthermore suggests that some of the terrestrial building materials are not present in our collections. Our data also imply that CAIs were not an important constituent of the Earth in agreement with Mg isotope evidence (Norman et al., 2006).

ACKNOWLEDGEMENTS

W. A. acknowledges support from the Science and Technology Facilities Council (UK) for the PhD studentship. The research leading to these results has received funding from the European Research Council under the European Union's Seventh Framework Programme (FP7/2007-2013)/ERC Grant agreement n° [279779]. This work was also supported by the Swiss National Science Foundation (Project 200021_149282). S. B. acknowledges financial support from the Joint Institute for Nuclear Astrophysics (JINA, University of Notre Dame, USA) and from the Karlsruhe Institute of Technology (KIT, Karlsruhe, Germany). We thank Caroline Smith (Natural History Museum, London), Linda Welzenbach (Smithsonian Institution National Museum of Natural History), Anne Kascak (Johnson Space Centre, Houston), Brigitte Zanda (National Museum of Natural History, Paris) and Philip Heck (Field Museum, Chicago) for the provision of meteorite samples. Mario Fischer-Gödde, Klaus Mezger and an anonymous referee are gratefully acknowledged for their constructive reviews, as is Munir Humayun for his thorough editorial handling, although they may not have shared the views expressed in this paper in their entirety.

REFERENCES

Akram W., Schönbächler M., Sprung P. and Vogel N. (2013) Zirconium-Hafnium isotope evidence from meteorite for the decoupled synthesis of light and heavy neutron-rich nuclei. *Astrophys. J.* **777**, 169–180.

Albarède F. (1996) *Introduction to Geochemical Modeling*. Cambridge University Press.

Alexander C. M. O'. D. (2005) Re–examining the role of chondrules in producing the elemental fractionations in chondrites. *Meteorit. Planet. Sci.* **40**, 943–965.

Amelin Y., Lee D.-C., Halliday A. N. and Pidgeon R. T. (1999) Nature of the Earth's earliest crust from hafnium isotopes in single detrital zircons. *Nature* **399**, 252–255.

Anders E. and Zinner E. (1993) Interstellar grains in primitive meteorites: diamond, silicon carbide, and graphite. *Meteoritics* **28**, 490–514.

Andreasen R. and Sharma M. (2006) Solar nebular heterogeneity in p–process samarium and neodymium isotopes. *Science* **314**, 806–809.

Andreasen R. and Sharma M. (2007) Mixing and homogenisation in the early solar system: clues from Sr, Ba, Nd, and Sm isotopes in meteorites. *Astrophys. J.* **665**, 874–883.

Arlandini C., Käppeler F., Wisshak K., Gallino R., Lugaro M., Busso M. and Straniero O. (1999) Neutron capture in low–mass asymptotic giant branch stars: cross sections and abundance signatures. *Astrophys. J.* **525**, 886–900.

Birck J.-L. (2004) An overview of isotopic anomalies in extraterrestrial materials and their nucleosynthetic heritage. *Rev. Mineral. Geochem.* **55**, 25–64.

Bisterzo S., Gallino R., Straniero O., Cristallo S. and Käppeler F. (2011a) The s-process in low-metallicity stars–I. *Mon. Not. R. Astron. Soc.* **404**, 1529–1544.

Bisterzo S., Gallino R., Straniero O., Cristallo S. and Käppeler F. (2011b) The s-process in low-metallicity stars–II. *Mon. Not. R. Astron. Soc.* **418**, 284–319.

Brandon A. D., Humayun M., Puchtel I. S., Leya I. and Zolensky M. (2005) Osmium isotope evidence for an s-process carrier in primitive chondrites. *Science* **309**, 1233–1236.

Burkhardt C., Kleine T., Oberli F., Pack A., Boudon B. and Wieler R. (2011) Molybdenum isotope anomalies in meteorites: constraints on solar nebula evolution and origin of the earth. *Earth Planet. Sci. Lett.* **312**, 390–400.

Burkhardt C., Kleine T., Dauphas N. and Wieler R. (2012) Origin of isotopic heterogeneity in the solar nebula by thermal processing and mixing of nebular dust. *Earth Planet. Sci. Lett.* **357**, 298–307.

Cameron A. G. W. and Truran J. W. (1977) The supernova trigger for the formation of the solar system. *Icarus* **30**, 447–461.

Cameron A. G. W. (1973) Abundances of the elements in the solar system. *Space Sci. Rev.* **15**, 121–146.

Carlson R. W., Boyet M. and Horan M. (2007) Chondrite barium, neodymium, and samarium isotopic heterogeneity and early earth differentiation. *Science* **316**, 1175–1178.

Chadwick M. B.47 other authors (2006) ENDF/B-VII.0: Next generated evaluated nuclear data library for nuclear science and technology. *Nucl. Data Sheets* **107**, 2931–3060.

Chen J. H., Papanastassiou D. A., Wasserburg G. J. and Ngo H. H. (2004) Endemic Mo isotopic anomalies in iron and carbonaceous meteorites. 35th Lunar and Planetary Science Conference. #1431 (abstr.).

Chen J. H., Papanastassiou D. A. and Wasserburg G. J. (2010) Ruthenium endemic isotope effects in chondrites and differentiated meteorites. *Geochim. Cosmochim. Acta* **74**, 3851–3862.

Chen H.-W., Lee T., Lee D.-C., Shen J. J.-S. and Chen J.-C. (2011) ^{48}Ca heterogeneity in differentiated meteorites. *Astrophys. J. Lett.* **743**, L23–L27.

Clayton R. N., Hinton R. W. and Davis A. M. (1988) Isotopic variations in the rock-forming elements in meteorites. *Phil. Trans. Roy. Soc. Lond. A* **325**, 483–501.

Clayton R. N. (1993) Oxygen isotopes in meteorites. *Ann. Rev. Earth Planet. Sci. Lett.* **21**, 115–149.

Clayton R. N. and Mayeda T. K. (1999) Oxygen isotope studies of carbonaceous chondrites. *Geochim. Cosmochim. Acta* **63**, 2089–2104.

Clayton D. (2003) *Handbook of the Isotopes*. Cambridge University Press.

Dauphas N., Marty B. and Reisberg L. (2002a) Molybdenum evidence for inherited planetary scale isotopic heterogeneity of the protosolar nebula. *Astrophys. J.* **565**, 640–644.

Dauphas N., Marty B. and Reisberg L. (2002b) Molybdenum nucleosynthetic dichotomy revealed in primitive meteorites. *Astrophys. J. Lett.* **569**, L139–L142.

Dauphas N., Davis A., Marty B. and Reisberg L. (2004) The cosmic molybdenum–ruthenium isotope correlation. *Earth Planet. Sci. Lett.* **226**, 465–475.

Dauphas N., Remusat L., Chen J. H., Roskosz M., Papanastassious D. A., Stodolna J., Guan Y., Ma C. and Eiler J. M. (2010) Neutron–rich chromium isotope anomalies in supernova nanoparticles. *Astrophys. J.* **720**, 1577–1591.

Davis A. M., Pellin M. J., Lewis R. S., Amari S. and Clayton R. N. (1999) Molybdenum and zirconium isotopic compositions of supernova grains. *Meteorit. Planet. Sci.* **34**, A30–A31.

Farouqi K., Kratz K.-L., Pfeiffer B., Rauscher T., Thielemann F.-K. and Truran J. W. (2010) Charged-particle and neutron–capture processes in the high-entropy wind of core–collapse supernovae. *Astrophys. J.* **712**, 1359–1377.

Fehr M. A., Rehkämper M., Halliday A. N., Schönbächler M., Hattendorf B. and Günther D. (2006) Search for nucleosynthetic and radiogenic tellurium isotope anomalies in carbonaceous chondrites. *Geochim. Cosmochim. Acta* **70**, 3436–3448.

Foster P. N. and Boss A. P. (1996) Triggering star formation with stellar eject. *Astrophys. J.* **468**, 784–796.

Goriely S. (2002) Hauser-Feshbach rates for neutron capture reactions. <http://www-astro.ulb.ac.be/Html/hfr.html. Version 9/12/2012>.

Hans U., Kleine T. and Bourdon B. (2013) Rb–Sr chronology of volatile depletion in differentiated protoplanets: BABI, ADOR and ALL revisited. *Earth Planet. Sci. Lett.* **374**, 204–214.

Harper C. L., Wiesmann H., Nyquist L. E., Hartmann D., Meyer B., Gallino R. and Raiteri C. M. (1991) Interpretation of the ^{50}Ti–^{96}Zr anomaly correlation in Allende CAI. 22nd Lunar and Planetary Science Conference. 517–518 (abstr.).

Hezel D. C., Russell S. S., Ross A. J. and Kearsley A. T. (2008) Modal abundances of CAIs: implications for bulk chondritic element abundances and fractionations. *Meteorit. Planet. Sci.* **43**, 1879–1894.

Huss G. R., Meshik A. P., Smith J. B. and Hohenberg C. M. (2003) Presolar diamond, silicon carbide, and graphite in carbonaceous chondrites: Implications for thermal processing in the solar nebula. *Geochim. Cosmochim. Acta* **67**, 4823–4848.

Jaeger M., Kunz R., Mayer A., Hammer J. W., Staudt G., Kratz M.-L. and Pfeiffer (2001) ^{22}Ne(alpha, n)^{25}Mg: the key neutron source in massive stars. *Phys. Rev. Lett.* **12**, 87–107.

Jones R. H., Lee T., Connolly H. C., Love S. G., and Shang H. (2000) Formation of chondrules and CAIs: theory vs. observation. In *Protostars and Planets IV* (eds. V. Mannings, A. P. Boss and S. S. Russell). University of Arizona Press, Tucson. pp. 927–962.

Käppeler F., Beer H. and Wisshak K. (1989) S-process nucleosynthesis – nuclear physics and the classical model. *Rep. Prog. Phys.* **52**, 945–1013.

Kastner J. H. and Myers P. C. (1994) An observational estimate of the probability of encounters between mass–losing evolved stars and molecular clouds. *Astrophys. J.* **421**, 605–614.

Kratz K.-L., Farouqi K., Mashonkina L. I. and Pfeiffer B. (2008) Nucleosynthesis modes in the high-entropy-wind of type II supernovae. *New Astron. Rev.* **52**, 390–395.

Krot A. N. and Keil K. (2002) Anorthite-rich chondrules in CR and CH carbonaceous chondrites: genetic link between calcium-aluminum-rich inclusions and ferromagnesian chondrules. *Meteorit. Planet. Sci.* **37**, 91–111.

Krot A. N., Hutcheon I. D. and Keil K. (2002) Plagioclase-rich chondrules in the reduced CV chondrites: Evidence for complex formation history and genetic links between calcium-aluminum-rich inclusions and ferromagnesian chondrules. *Meteorit. Planet. Sci.* **37**, 155–182.

Krot A. N., Fagan T. J., Keil K., McKeehan K. D., Sahijpal S., Hutcheon I. D., Petaev M. I. and Yurimoto H. (2004) Ca, Al-rich inclusions, amoeboid olivine aggregates, and Al-rich chondrules from the unique carbonaceous chondrite Acfer 094. *Geochim. Cosmochim. Acta* **68**(9), 2167–2184.

Lauretta, D. and McSween, H. (eds.) (2006) *Meteorites and the Early Solar System II*. University of Arizona Press.

Lee D.-C. and Halliday A. N. (2000) Accretion of primitive planetesimals: Hf-W isotopic evidence from enstatite chondrites. *Science* **288**, 1629–1631.

Lee T., Papanastassiou D. A. and Wasserburg (1976) Demonstration of ^{26}Mg excess in Allende and evidence for ^{26}Al. *Geophys. Res. Lett.* **3**, 109–112.

Le Guillou C., Bernard S., Brearley A. J. and Remusat L. (2014) Evolution of organic matter in Orgueil, Murchison Renazzo during parent body aqueous alteration: In situ investigations. *Geochim. Cosmochim. Acta* **131**, 368–392.

Leya I., Schönbächler M., Wiechart U., Krahenbuhl U. and Halliday A. N. (2008) Titanium isotopes and the radial heterogeneity of the solar system. *Earth Planet. Sci. Lett.* **266**, 233–244.

Leya I., Schönbächler M., Krahenbuhl U. and Halliday A. N. (2009) New titanium isotope data for Allende and Efremovka CAIs. *Astrophys. J.* **702**, 1118–1126.

Lodders K. (2003) Solar system abundances and condensation temperatures of the elements. *Astrophys. J.* **591**, 1220–1247.

Lodders K., Palme H. and Gail H.-P. (2009) Abundances of the elements in the solar system. In *Landolt-Börnstein New series, Vol. VI/4B, Chap 4.4*, Springer-Verlag, 560–630.

Lugaro M., Davis A. M., Gallino R., Pellin M. J., Straniero O. and Käppeler F. (2003) Isotopic compositions of strontium, zirconium, molybdenum, and barium in single presolar SiC grains and asymptotic giant branch stars. *Astrophys. J.* **593**, 486–508.

Lugmair G. W. and Shukolyukov A. (2001) Early solar system events and timescales. *Meteorit. Planet. Sci.* **36**, 1017–1026.

Mason B. and Taylor S. R. (1982) Inclusions in the Allende meteorite. *Smithson. Contrib. Earth Sci.* **25**, 1–40.

McDonough W. F. (2001) The composition of the Earth. In *Earthquake thermodynamics and phase transformations in the earths interior*. Edited by Teisseyre R. and Majewski E. 76, Academic Press, pp. 3–23.

Meyer B., Clayton D. D. and The L. S. (2000) Molybdenum and zirconium isotopes from a supernova neutron blast. *Astrophys. J. Lett.* **540**, 49–52.

Minster J. F. and Allègre C. J. (1982) The isotopic composition of zirconium in terrestrial and extraterrestrial samples: implications for extinct ^{92}Nb. *Geochim. Cosmochim. Acta* **46**, 565–573.

Moynier F., Dauphas N. and Podesek F. A. (2009) A search for ^{70}Zn anomalies in meteorites. *Astrophys. J. Lett.* **700**, 92–95.

Moynier F., Agranier A., Hezel D. C. and Bouvier A. (2010) Sr stable isotope composition of the Earth, the Moon, Mars, Vesta and meteorites. *Earth Planet. Sci. Lett.* **300**, 359–366.

Nicolussi G. K., Davis A. M., Pellin M. J., Lewis R. S., Clayton R. N. and Amari S. (1997) S-process Zirconium in presolar silicon carbide grains. *Science* **277**, 1281–1283.

Niemeyer S. and Lugmair G. W. (1984) Titanium isotopic anomalies in meteorites. *Geochim. Cosmochim. Acta* **48**, 1401–1416.

Norman M. D., Yaxley G. M., Bennett V. C. and Brandon A. D. (2006) Magnesium isotopic composition of olivine from the Earth, Mars, Moon, and pallasite parent body. *Geophys. Res. Lett.* **33**, L15202.

Podosek F. A., Ott U., Brannon J. C., Neal C. R., Bernatowicz T. J., Swan P. and Mahan S. E. (1997) Thoroughly anomalous chromium in Orgueil. *Meteorit. Planet. Sci.* **32**, 617–627.

Qian Y.-Z. and Wasserburg G. J. (2007) Where, oh where has the r-process gone? *Phys. Rep.* **442**, 237–268.

Qin L., Nittler L. R., Alexander C. M. O'. D., Wang J., Stadermann F. J. and Carlson R. W. (2011) Extreme ^{54}Cr–rich nano–oxides in the CI chondrite Orgueil – implication for a late supernova injection into the solar system. *Geochim. Cosmochim. Acta* **75**, 629–644.

Quitté G., Halliday A. N., Meyer B. S., Markowski A., Latkoczy C. and Günther D. (2007) Correlated iron-60, nickel-62, and zirconium-96 in refractory inclusions and the origin of the solar system. *Astrophys. J.* **655**, 678–682.

Raiteri C. M., Gallino R., Busso M., Neuberger D. and Käppeler F. (1993) The weak s-component and nucleosynthesis in massive stars. *Astrophys. J.* **419**, 207–223.

Ranen M. C. and Jacobsen S. B. (2006) Barium isotopes in chondritic meteorites: implications for planetary reservoir models. *Science* **314**, 809–812.

Regelous M., Elliott T. and Coath C. D. (2008) Nickel isotope heterogeneity in the early solar system. *Earth Planet. Sci. Lett.* **272**, 330–338.

Reisberg L., Dauphas N., Luguet A., Pearson D. G., Gallino R. and Zimmerman C. (2009) Nucleosynthetic osmium isotope anomalies in acid leachates of the Murchison meteorite. *Earth Planet. Sci. Lett.* **277**, 334–344.

Rotaru M., Birck J. L. and Allègre C. J. (1992) Clues to early solar system history from chromium isotopes in carbonaceous chondrites. *Nature* **358**, 465–470.

Schönbächler M., Rehkämper M., Halliday A. N., Lee D.-C., Bourot-Denise M., Zanda B., Hattendorf B. and Günther D. (2002) Niobium-zirconium chronometry and early solar system development. *Science* **295**, 1705–1708.

Schönbächler M., Lee D.-C., Rehkämper M., Halliday A. N., Fehr M. A., Hattendorf B. and Günther D. (2003) Zirconium isotope evidence for incomplete admixing of r–process components in the solar nebula. *Earth Planet. Sci. Lett.* **216**, 467–481.

Schönbächler M., Rehkämper M., Lee D.-C. and Halliday A. N. (2004) Ion exchange chromatography and high precision isotopic measurements of zirconium by MC–ICPMS. *Analyst* **129**, 32–37.

Schönbächler M., Rehkämper M., Fehr M. A., Halliday A. N., Hattendorf B. and Günther D. (2005) Nucleosynthetic zirconium isotope anomalies in acid leachates of carbonaceous chondrites. *Geochim. Cosmochim. Acta* **69**, 5113–5122.

Schönbächler M., Carlson R. W., Horan M. F., Mock T. D. and Hauri E. H. (2010) Heterogeneous accretion and the moderately volatile element budget of earth. *Science* **328**, 884–887.

Schönbächler M., Akram W. M., Williams N. H. and Leya I. (2011) Nucleosynthetic heterogeneities of neutron–rich isotopes in calcium aluminium–rich inclusions and bulk solar system materials. Formation of the First Solids in the Solar System. #9085.

Scott E. R. D. and Krot A. N. (2007) Chondrites and their components. In *Meteorites, Comets and Planets* (ed. A. M. Davis) Chapter 1.07, Treatise on Geochemistry Update, Elsevier.

Shibata K.23 other authors (2002) Japanese evaluated nuclear data library version 3 revision 3: JENDL-3.3. *Nucl. Sci. Technol.* **39**, 1125–1136.

Simon J. I., DePaolo D. J. and Moynier F. (2009) Calcium isotope composition of meteorites, Earth and Mars. *Astrophys. J.* **702**, 707–715.

Sprung P., Scherer E. E., Upadhyay D., Leya I. and Mezger K. (2010) Non–nucleosynthetic heterogeneity in non–radiogenic stable Hf isotopes: implications for early solar system chronology. *Earth Planet. Sci. Lett.* **295**, 1–11.

Steele R. C. J., Coath C. D., Regelous M., Russell S. and Elliott T. (2012) Neutron-poor Nickel isotope anomalies in meteorites. *Astrophys. J.* **758**, 59–80.

Toukan K. A. and Käppeler F. (1990) The stellar neutron capture cross sections of ^{94}Zr and ^{96}Zr. *Astrophys. J.* **348**, 357–362.

Travaglio C., Gallino R., Arnone R., Cowan J., Jordan F. and Snedon C. (2004) Galactic evolution of Sr, Y, Zr: a multiplicity of nucleosynthetic processes. *Astrophys. J.* **601**, 864–884.

Travaglio C., Ropke F. K., Gallino R. and Hillebrandt W. (2011) Type Ia supernovae as sites of the p-process: two-dimensional models coupled to nucleosynthesis. *Astrophys. J.* **739**, 93–112.

Trinquier A., Birck J.-L. and Allègre C. J. (2007) Widespread ^{54}Cr heterogeneity in the inner solar system. *Astrophys. J.* **655**, 1179–1185.

Trinquier A., Elliott T., Ulfbeck D., Coath C., Krot A. N. and Bizzarro M. (2009) Origin of nucleosynthetic isotope heterogeneity in the solar protoplanetary disk. *Science* **324**, 374–376.

Van Acken D., Brandon A. D. and Humayun M. (2011) High–precision osmium isotopes in enstatite and Rumuruti chondrites. *Geochim. Cosmochim. Acta* **75**, 4020–4036.

Wasserburg G. J. and Qian Y.-Z. (2009) Chemical evolution of the juvenile universe. *Publ. Astron. Soc. Austral.* **26**, 184–193.

Wiechert U., Halliday A. N., Lee D.-C., Snyder G. A., Taylor L. A. and Rumble D. (2001) Oxygen isotopes and the moon-forming giant impact. *Science* **294**, 345–348.

Williams N. H., Schönbächler M., Fehr M. A., Akram W. M. and Parkinson I. J. (2014) Different heterogeneously distributed titanium isotope components in solar system materials and mass-dependant titanium isotope variations. 45th Lunar and Planetary Science Conference. ♯ 2183 (abstr.).

Yokoyama T., Rai V. K., Alexander C. M. O. 'D., Lewis R. S., Carlson R. W., Shirley S. B., Thiemens M. H. and Walker R. J. (2007) Osmium isotope evidence for uniform distribution of s- and r-process components in the early solar system. *Earth Planet. Sci. Lett.* **259**, 567–580.

Yokoyama T., Alexander C. M. O. 'D. and Walker R. J. (2010) Osmium isotope anomalies in chondrites: results for acid residues and related leachates. *Earth Planet. Sci. Lett.* **291**, 48–59.

Zhang J., Dauphas N., Davis A. M., Leya I. and Fedkin A. (2012) The proto-earth as a significant source of lunar material. *Nat. Geosci.* **5**, 251–255.

Zinner E., Nittler L. R., Hoppe P., Gallino R., Straniero O. and Alexander C. M. O. 'D. (2005) Oxygen, magnesium and chromium isotopic ratios of presolar spinel grains. *Geochim. Cosmochim. Acta* **69**, 4149–4165.

Associate Editor: Munir Humayun